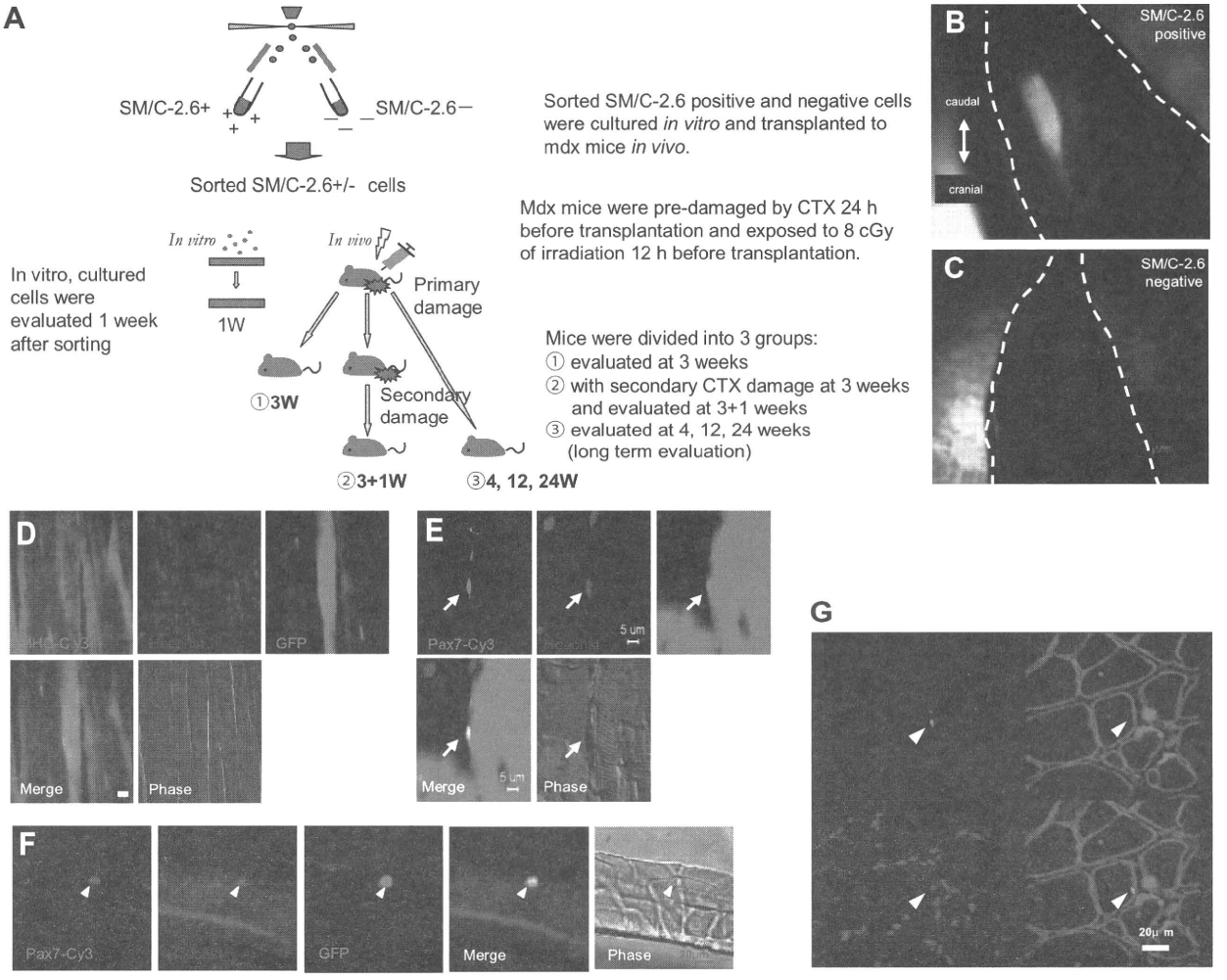

Figure 4. ES-derived satellite-like cells can repair damaged muscle *in vivo*. *A*) Methods for *in vitro* and *in vivo* analysis of sorted SM/C-2.6-positive and -negative cells derived from mES cells. *B, C*) ES-derived GFP-positive tissue engrafted to the LTA muscle of a recipient mouse that received SM/C-2.6-positive cells (*B*) but SM/C-2.6-negative cells (*C*). *D*) Grafted GFP-positive tissues were histologically MHC positive. *E*) GFP/Pax7-double-positive cells were observed in mice that received SM/C-2.6-positive cells by anti-Pax7 immunostaining. *F*) GFP/Pax7-double-positive cells were also confirmed by immunostaining of isolated single fibers. *G*) Laminin immunostaining indicated that the GFP-positive cells were located between the basal lamina and the muscle cell plasma membrane, which is consistent with the anatomical definition of muscle satellite cells. Scale bars = 1 mm (*B, C*); 15 μm (*D*); 5 μm (*E*); 20 μm (*F, G*).

(Fig. 4*G*). In contrast, in mice transplanted with SM/C-2.6-negative cells, GFP-positive tissues were rarely observed, and none of the GFP-positive cells were positive for skeletal MHC. H&E staining indicated that these GFP-positive tissues were surrounded by inflammatory cells (Supplemental Fig. 8), suggesting that these nonmyogenic tissues may undergo phagocytosis. These results demonstrate that ES-derived SM/C-2.6-positive satellite-like cells could be engrafted *in vivo* and repair damaged muscle tissues of the host.

Engrafted ES-derived satellite-like cells function as satellite cells following muscle damage

Muscle satellite cells are generally considered to be self-renewing monopotent stem cells that differentiate into myoblasts and myofibers to repair damaged skeletal muscles. To determine whether these engrafted GFP^+ES-derived satellite-like cells are functional stem cells, we injured the LTA muscle of primary recipient mice 3 wk after primary transplantation with GFP^+SM/C-2.6-positive cells. This experiment let us assess the ability of satellite-like cells to repair damaged muscle fibers and self-renew *in vivo* (14). The LTA muscles were removed and analyzed 1 wk after the secondary injury (reinjured group). Mice that were initially injected with GFP^+SM/C-2.6-positive cells without a second injury were used as a control (nonreinjured group). These control mice were analyzed 3 or 4 wk after transplantation (Fig. 4*A*). GFP-positive muscle fascicles were counted in sections of both reinjured and nonreinjured muscle (**Fig. 5*A, B***). In the reinjured group 461.7 ± 117.4 (n=6; per view, ×100) GFP-positive muscle fascicles were observed. In comparison, only 136.7 ± 27.9 (n=4) and 168.7 ± 72.9 (n=6; per view, ×100) GFP-positive muscle fascicles were evident in

TABLE 1. *Transplantation of reinjured and nonreinjured mice and long-term evaluation*

Group	TA with GFP$^+$ fascicles [n(%)][a]	Mouse	Cells/TA injected (n)	GFP$^+$ fascicles/TA (avg)[b]	GFP$^+$/Pax7$^+$ cells/TA (avg)[c]	Engraftment efficiency
SM/C-2.6$^+$						
3W	4/8 (50%)	1	1.75×10^4	125.3	5.3	
		2	3.5×10^4	111.1	7.1	
		3	5×10^4	134.2	5.1	
		4	8×10^4	176.1	4.2	
Mean			$4.5 \pm 2.6 \times 10^4$	136.7 ± 27.0	5.4 ± 1.2	0.30%
4W	6/9 (66.67%)	1	2×10^4	77.3	6.1	
		2	1.3×10^5	153.2	4.6	
		3	5×10^4	163.1	6.8	
		4	3.5×10^4	168.9	5.1	
		5	8×10^4	281.1	7.2	
		6	1.75×10^4	169.4	6.2	
Mean			$3.6 \pm 2.5 \times 10^4$	168.7 ± 72.9	6 ± 1	0.47%
3 + 1W	6/8 (75%)	1	2×10^4	581.2	11.2	
		2	1.3×10^5	370.3	11.5	
		3	5×10^4	586.6	10.1	
		4	3.5×10^4	486.6	5.9	
		5	8×10^4	347.1	15.3	
		6	1.75×10^4	542.9	10.8	
Mean			$5.5 \pm 4.3 \times 10^4$	461.7 ± 117.3	10.8 ± 3	0.84%
12W	3/5 (60%)	1	2×10^4	391.5	9.7	
		2	5×10^4	266	9.3	
		3	8×10^4	280.2	6	
Mean			$5 \pm 3 \times 10^4$	312.6 ± 68.7	8.3 ± 2	0.59%
24W	1/2 (50%)	1	2×10^4	58.62	3.45	
Mean			2×10^4	58.62	3.45	0.20%
SM/C-2.6$^-$						
3W	0/8 (0%)	1–8	$1–8 \times 10^4$	0	0	0%
4W	0/9 (0%)	1–9	$1.3–8 \times 10^4$	0	0	0%
3 + 1W	0/8 (0%)	1–8	$1.75–13 \times 10^4$	0	0	0%
12W	0/5 (0%)	1–8	$2–8 \times 10^4$	0	0	0%
24W	0/2 (0%)	1–2	2×10^4	0	0	0%

Serial transplantation

	Primary transplantation		Secondary transplantation		
Mouse	Cells injected	Collected GFP$^+$ cells/TA	Cells injected	GFP$^+$ fascicles/TA	Engraftment efficiency
1	2×10^4	3253	200	29.3	14.7%
2	2×10^4	2277	200	28.6	14.3%
Mean	2×10^4	2765	200	29 ± 0.5	14.5%

TA, tibialis anterior; 3W, nonreinjured group analyzed 3 wk after cell transplantation; 4W, nonreinjured group analyzed 4 wk after cell transplantation; 3 + 1W, reinjured group reinjured 3 wk after cell transplantation and analyzed 1 wk after reinjury; 12W, long-term engraftment evaluation analyzed 12 wk after cell transplantation; 24W, long-term engraftment evaluation analyzed 24 wk after cell transplantation. [a]Percentage of TA that had engrafted with GFP$^+$ fibers was calculated as number of TAs with GFP$^+$ fibers/total TAs injected with cells. [b]Average determined from number of GFP$^+$ muscle fascicles counted per field at ×100 in 10 fields. [c]Average determined from number of GFP$^+$/Pax7+ cells counted per field at ×100 in 10 fields.

the nonreinjured groups at 3 and 4 wk, respectively, after transplantation (Fig. 5*B* and Table 1). Furthermore, we also observed that many GFP-positive muscle fibers had a typical central nucleus in the reinjured group (Fig. 5*C*), indicating regenerating muscle fibers. Taken together, these results suggest that these GFP-positive muscle tubes were freshly regenerated by the engrafted GFP$^+$ ES-derived satellite-like cells in response to the second injury. Surprisingly, immunostaining with anti-Pax7 revealed an increase in number of GFP/Pax7-double-positive cells in the reinjured group (10.8±3.0/view compared to 5.4±1.2, and 6.0±1.0 in the nonreinjured group; Fig. 5*D* and Table 1). This result strongly suggests that engrafted ES-derived satellite-like cells not only self-renewed but also expanded in number, possibly replacing the recipient satellite cells lost because of excessive repair of skeletal muscle in response to the second injury.

ES-derived satellite-like cells are capable of long-term engraftment in recipient muscles

Long-term engraftment is an important characteristic of self-renewing stem cells. If these ES-derived satellite-

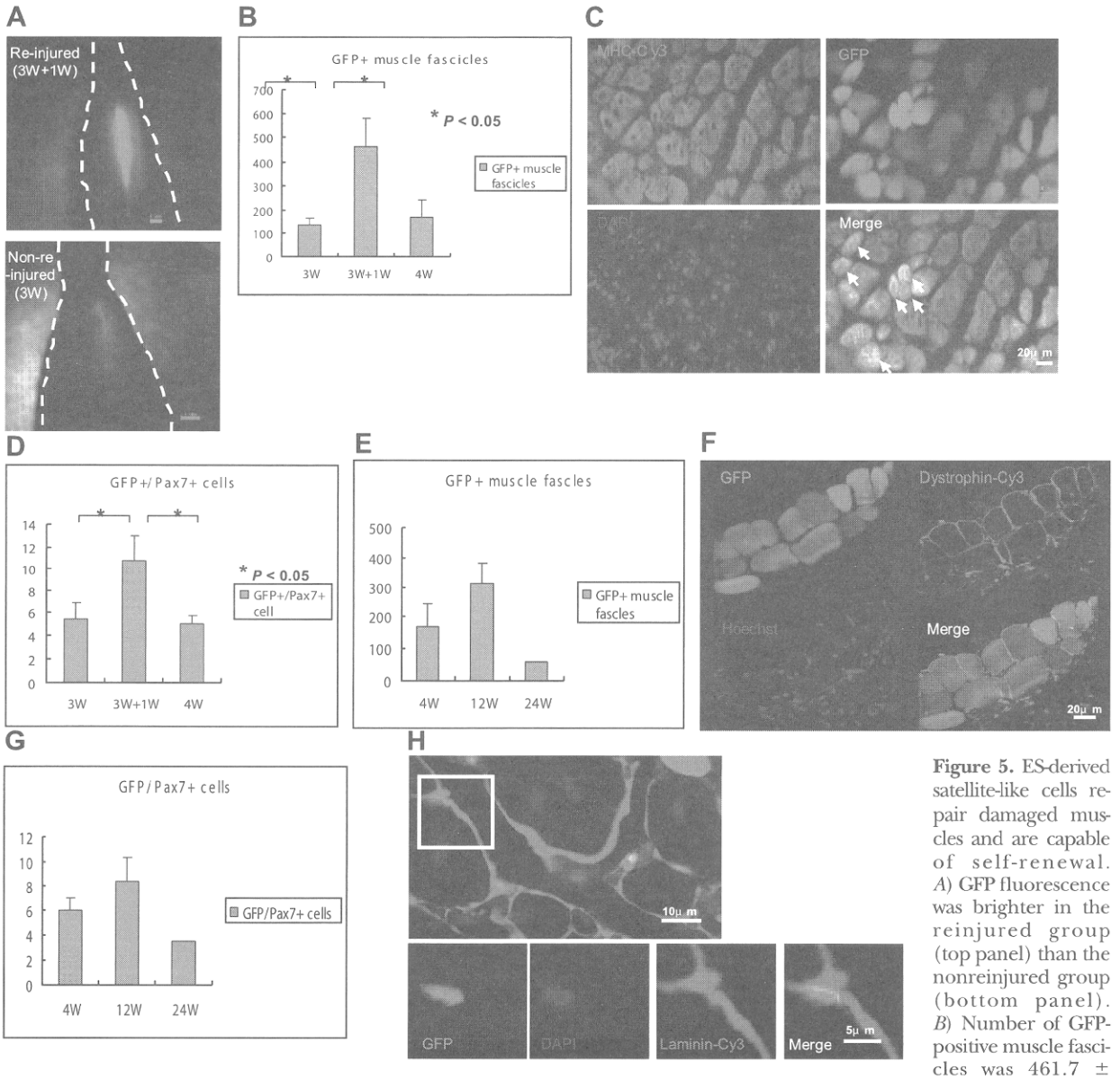

Figure 5. ES-derived satellite-like cells repair damaged muscles and are capable of self-renewal. *A*) GFP fluorescence was brighter in the reinjured group (top panel) than the nonreinjured group (bottom panel). *B*) Number of GFP-positive muscle fascicles was 461.7 ± 117.3 in the reinjured group (3W+1W) and 136.7 ± 27.9 and 168.7 ± 72.9 in the nonreinjured group at 3 wk (3W) and 4 wk (4W), respectively. *C*) GFP-positive fibers were confirmed to be MHC positive and contained central nuclei (arrows). *D*) Number of GFP/Pax7-double-positive cells also increased significantly in the reinjured group (10.8±3.0 cells at 3W+1W) compared to the nonreinjured group (5.4±1.2 and 6.0±1.0 at 3W and 4W, respectively). *E*) In long-term evaluations, number of GFP-positive muscle fascicles at 12 wk (12W) increased relative to number at 4 wk after transplantation [312.6±68.7 (n=3) *vs.* 168.7±72.9]. However, a decrease was observed at 24 wk (58.6; n=1). *F*) Immunostaining showed dystrophin (red) surrounding the donor-derived GFP-positive fibers (green), 24 wk after transplantation of SM/C-2.6-positive cells. *G*) Results similar to *E* were observed with the number of GFP/Pax7-double-positive cells. *H*) A GFP-positive cell beneath the basal lamina was observed. Scale bars = 1 mm (*A*); 20 μm (*C*); 20 μm (*F*); 10 μm (*H*, top panel); 5 μm (*H*, bottom panels).

like cells function as normal stem cells in skeletal muscle, they should be able to reside within the tissue for long periods of time and undergo asymmetric cell divisions to maintain the number of satellite cells and to generate muscle fibers. To examine this stem cell function, we analyzed the recipient mice at 4, 12, and 24 wk after transplantation. Intriguingly, in the LTA muscle of mdx mice transplanted with SM/C-2.6-positive cells, the number of GFP-positive fascicles at 12 wk increased over that at 4 wk [12.6±68.7 (n=3) *vs.* 168.7±72.9; Fig. 5*E*] but decreased by 24 wk (58.6; n=1). These engrafted GFP-positive tissues were confirmed to be MHC positive through immunostaining (Supplemental Fig. 9), and surrounding these GFP-positive fibers, dystrophin was observed (Fig. 5*F*). The numbers of GFP/Pax7-double-positive cells were maintained from week 4 to week 24 (Fig. 5*G*, Table 1, and Supplemental Fig. 10) and the location of GFP-positive cells under the basal lamina meets the anatomical definition of satellite cells (Fig. 5*H*). No teratomas were

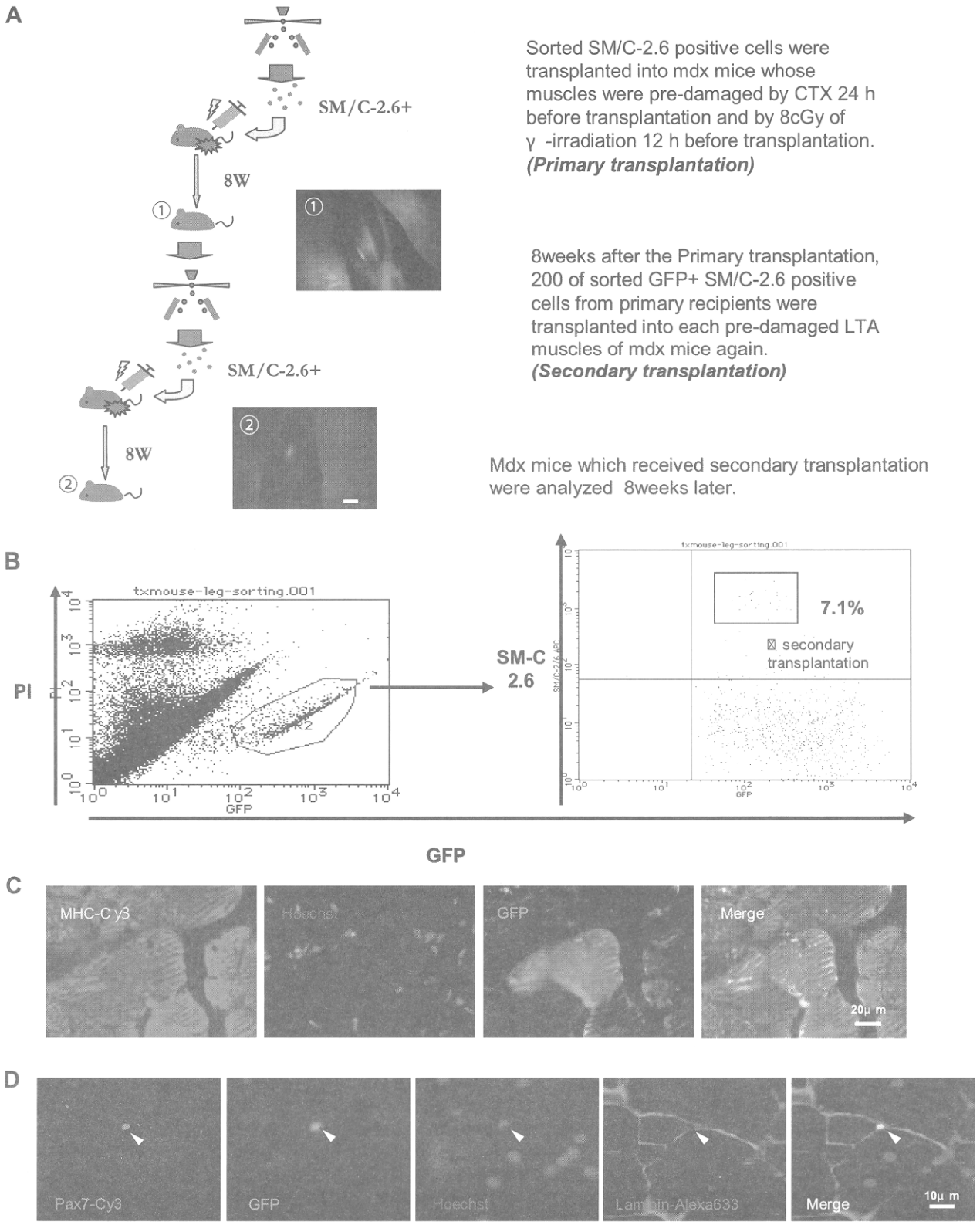

Figure 6. ES-derived satellite-like cells can be secondarily transplanted. *A*) SM/C-2.6-positive cells (2.5×10^4) were transplanted into the LTA muscle of recipient mice in primary transplantation, and as few as 200 SM/C-2.6-positive cells collected from the primary recipients were retransplanted (secondary transplantation) into the LTA muscle of secondary recipient mice. *B*) FACS data of primary transplantation indicated that 7.1% of engrafted (GFP-positive) cells were SM/C-2.6-positive. *C*) Eight weeks after secondary transplantation, immunostaining of LTA muscle for MHC showed that engrafted ES-derived GFP-positive tissues formed mature skeletal muscle fibers. *D*) GFP/Pax7-double-positive cells (arrowhead) located beneath the basal lamina were observed within GFP-positive LTA muscle of secondary recipient mice. Scale bars = 2 mm (*A*); 20 μm (*C*); 10 μm (*D*).

found in recipient mice transplanted with SM/C-2.6-positive cells. Thus, ES-derived satellite-like cells effectively engrafted and provided long-term stem cells, which played an important role in maintenance of the integrity of the surrounding muscle tissue.

ES-derived satellite-like cells can be secondarily transplanted

For a more thorough characterization of the ES-derived satellite-like cells, we performed serial transplantations. Eight weeks after the primary cell transplantation with 2×10^4 SM/C-2.6-positive cells, the LTA muscles of the primary recipient mice were dissected to isolate the engrafted ES-derived cells, 2765 ± 685.9 (n=2; **Fig. 6*A***). The GFP^+/SM/C-2.6-positive cells within the engrafted cells were sorted by FACS (204±33.9; n=2), and only 200 GFP+/SM/C-2.6-positive cells/mouse were transplanted into predamaged LTA muscles of mdx mice (Fig. 6*B*). Eight weeks later (16 wk after the primary transplantation), the recipient mice were analyzed. GFP-positive tissue in the LTA muscle of the secondary recipient mice was observed (Fig. 6*A*). The GFP-positive tissues were confirmed to be MHC-positive mature skeletal muscle (Fig. 6*C*), and surrounding these engrafted GFP-positive skeletal muscle fascicles, dystrophin was observed (Supplemental Fig. 11). GFP/Pax7-double-positive cells located beneath the basal lamina were also detected in the engrafted tissue (Fig. 6*D*). Thus, with only 200 GFP^+SMC/2.6-positive cells, injured skeletal muscle and Pax7+ cells were successfully restored in the secondary recipients. These findings demonstrate that stem cell fraction contained within SM/C-2.6-positive cells was enriched *in vivo* through transplantation.

DISCUSSION

Many attempts have been made to induce mES cells into the skeletal muscle lineage, with hanging drop cultures for EB formation being the most widely applied method (25). However, although EBs contain cells derived from all 3 germ layers, effective induction of mES cells into the myogenic lineage, including myogenic stem cells (satellite cells), has not yet been achieved. Because of the lack of adequate surface markers, purifying ES-derived myogenic precursor/stem cells from differentiated mES cells *in vitro* has been difficult. To overcome these problems, we modified the classic EB culture system by combining it with aspects of the single-fiber culture method. Single-fiber culture (33) has been used for functional evaluation of satellite cells. When a single myofiber is plated on a Matrigel-coated plate with DMEM containing HS, satellite cells migrate out of the fiber and differentiate into myoblasts to form myofibers *in vitro*. Matrigel allows the migrating satellite cells to proliferate before differentiating and fusing into large multinucleated myotubes (35). We hypothesized that this Matrigel environment might be suitable for ES cell differentiation into satellite cells and myoblasts. Therefore, we introduced Matrigel and HS into the classic EB culture system and established an efficient induction system for myogenic lineage cells, including cells expressing Pax7, a commonly recognized marker for skeletal muscle stem cells. Furthermore, we also successfully enriched ES-derived Pax7-positive myogenic precursor/stem cells using the SM/C-2.6 antibody.

The steps in ES cell induction are thought to be homologous to normal embryogenesis. During normal skeletal myogenesis, the initial wave of myogenic precursor cells in the dermomyotome express Myf5/MRF4 and Pax3, followed by a wave of Pax3/Pax7 expression (36). These waves of myogenesis act upstream of the primary myogenic transcription factor MyoD (37-39). In myotome formation skeletal myogenesis begins with myoblasts, termed somitic myoblasts, which appear at approximately E8.5, followed by the appearance of embryonic myoblasts (E11.5), fetal myoblasts (E16.5), and, ultimately, satellite cells, which are responsible for postnatal muscle regeneration (40). Our RT-PCR results (Fig. 1*J*) showed an earlier appearance of Pax3 expression, on d 3 + 3, followed by Pax3/Pax7 expression on d 3 + 3 + 7 and stronger expression of Pax3 than Pax7. These results resemble normal myogenesis, in which the primary wave of myogenesis is followed by a secondary wave of Pax3/Pax7-dependent myogenesis (41). Considering that in the time course of myogenesis satellite cells emerge during late fetal development, ES-derived Pax7-positive cells were collected on d 3 + 3 + 14 in an attempt to acquire cells that correspond to those of the late fetal to neonatal period. However, RT-PCR results of myogenic factors in SM/C-2.6-positive cells (Fig. 2*B*) indicated that these ES-derived SM/C-2.6-positive cells are a heterogeneous population, because they express not only Pax3 and Pax7 but also Myf5 and c-met. Although further confirmation is needed, we hypothesize that both embryonic/fetal myoblasts expressing Myf-5 and/or c-met and satellite/long-term stem cells expressing Pax3/Pax7 are present.

To confirm that the ES-derived SM/C-2.6-positive cell population contained functional satellite cells, the muscle regeneration and self-renewal capacities were examined. Recently Collins *et al.* established an excellent system in which sequential damage to the muscle of a recipient mouse was applied, to evaluate both muscle regeneration and self-renewal (14) Using their experimental approach, a significant increase in numbers of both ES-derived GFP-positive muscle fascicles and GFP/Pax7-double-positive cells was observed in mice that received a second injury. This result not only demonstrates the myogenic ability of ES-derived cells but also strongly supports the idea that these cells undergo self-renewal *in vivo*.

Analysis of long-term engraftment is an important method to verify self-renewal ability, for 2 reasons. First, ES-derived satellite cells must be able to engraft for long periods of time in order to provide the amount of progeny needed for repairing damaged tissue for an

extended period. In our study the ES-derived GFP-positive skeletal muscle tissues and Pax7-positive cells engrafted up to 24 wk and were located beneath the basal lamina, which is consistent with the anatomical definition of satellite cells. Although the number of GFP-positive fascicles at 24 wk decreased compared to 12 wk, this diminution may be due to the heterogeneity of ES-derived SM/C-2.6-positive cells as we mentioned. Because myoblasts cannot support myogenesis in the long term, we believe that GFP-positive fascicles at 24 wk are products of ES-derived satellite-like cells. Second, one of the potential risks of ES cell transplantation is teratoma formation. Considering clinical applications, it is extremely important to prevent formation of teratomas in the recipients. In our study more than 60 transplanted mice were evaluated through gross morphological and histological examination. There were no teratomas formed in mice that received SM/C-2.6-positive cells, and only 1 teratoma was found among the mice that received SM/C-2.6-negative cells. This result suggests that the risk of tumor formation by the ES cells was eliminated by using sorted SM/C-2.6-positive cells.

In addition to the sequential damage model and the long-term engraftment evaluation, we performed serial transplantations to further confirm the stem cell properties of these ES-derived SM/C-2.6-positive cells. Serial transplantation enables the identification and separation of long-term stem cells from short-term progenitors (42). To eliminate myoblast involvement, we designed a serial transplantation protocol of 8 + 8 wk (*i.e.*, a second transplantation 8 wk after the primary transplantation and an analysis of recipient mice 8 wk after the second transplantation). Strikingly these recollected ES-derived SM/C-2.6-positive cells showed significantly higher engraftment efficiency compared to the primary transplantation. In the previous reports engraftment efficiencies of myoblasts transplantation was ~0.1-0.2%, with the highest reported value being 2% (43-45). This engraftment efficiency is similar to our primary transplantation (0.2-0.8%) as well as the plating efficiency of SM/C-2.6-positive cells *in vitro* (0.07%). In our study as few as 200 recollected ES-derived SM/C-2.6-positive cells were transplanted in the second transplantation, and 29.0 ± 0.47 (n=2) fascicles were observed, which indicates 14.7% of higher engraftment efficiency. Thus, through the serial transplantation, ES-derived stem cell fraction was purified. A comparison of these SM/C-2.6-positive cells before and after injection might help to characterize the stem cell fraction derived from ES cells.

There have been few reports describing transplantation of ES-derived myogenic cells into injured muscles, and the report of engraftable skeletal myoblasts derived from human ES cells represents significant progress (26). Recently Darabi *et al.* (46) have reported that by introducing Pax3 into mouse embryoid bodies, autonomous myogenesis was initiated *in vitro*, and Pax3-induced cells regenerated skeletal muscles *in vivo* by sorting the PDGF-a+Flk-1- cells. The Pax3 expression was not observed until 7 d of differentiation culture, but introduced Pax3 expression pushed EBs to myogenic differentiation. Interestingly, we observed Pax3 expression at d 3 + 3 weakly and d 3 + 3 + 7 strongly, and gene expression process in our culture is very similar to theirs. In prolonged culture using Matrigel and HS, EBs were able to initiate myogenesis without gene modification in our system.

In conclusion, we successfully generated transplantable myogenic cells, including satellite-like cells, from mES cells. The ES-derived myogenic precursor/stem cells could be enriched using a novel antibody, SM/C-2.6. These ES-derived SM/C-2.6-positive cells possess a high myogenic potential, participate in muscle regeneration, and are located beneath the basal lamina where satellite cells normally reside. The self-renewal of these ES-derived satellite-like cells enabled them to survive long-term engraftment, up to 24 wk. Through serial transplantation, these ES-derived SM/C-2.6-positive cells were further enriched and produced a high engraftment efficiency of 14.7%.

Our success in inducing mES cells to form functional muscle stem cells, the satellite-like cells, will provide an important foundation for clinical applications in the treatment of DMD patients. FJ

This work was supported by a Grant-in-Aid for Scientific Research (S) (19109006) and a Grant-in-Aid for Scientific Research (B) (18390298) from the Ministry of Education, Science, Technology, Sports, and Culture of Japan.

REFERENCES

1. Nawrotzki, R., Blake, D. J., and Davies, K. E. (1996) The genetic basis of neuromuscular disorders. *Trends Genet.* **12,** 294–298
2. Emery, A. E. (2002) The muscular dystrophies. *Lancet* **359,** 687–695
3. Michalak, M., and Opas, M. (1997) Functions of dystrophin and dystrophin associated proteins. *Curr. Opin. Neurol.* **10,** 436–442
4. Suzuki, A., Yoshida, M., Hayashi, K., Mizuno, Y., Hagiwara, Y., and Ozawa, E. (1994) Molecular organization at the glycoprotein-complex-binding site of dystrophin. Three dystrophin-associated proteins bind directly to the carboxy-terminal portion of dystrophin. *Eur. J. Biochem./FEBS* **220,** 283–292
5. Bonilla, E., Samitt, C. E., Miranda, A. F., Hays, A. P., Salviati, G., DiMauro, S., Kunkel, L. M., Hoffman, E. P., and Rowland, L. P. (1988) Duchenne muscular dystrophy: deficiency of dystrophin at the muscle cell surface. *Cell* **54,** 447–452
6. Mauro, A. (1961) Satellite cell of skeletal muscle fibers. *J. Biophys. Biochem. Cytol.* **9,** 493–495
7. Moss, F. P., and Leblond, C. P. (1971) Satellite cells as the source of nuclei in muscles of growing rats. *Anat. Rec.* **170,** 421–435
8. Snow, M. H. (1978) An autoradiographic study of satellite cell differentiation into regenerating myotubes following transplantation of muscles in young rats. *Cell Tissue Res.* **186,** 535–540
9. Jejurikar, S. S., and Kuzon, W. M., Jr. (2003) Satellite cell depletion in degenerative skeletal muscle. *Apoptosis* **8,** 573–578
10. Schultz, E., and Jaryszak, D. L. (1985) Effects of skeletal muscle regeneration on the proliferation potential of satellite cells. *Mech. Ageing Dev.* **30,** 63–72
11. Webster, C., and Blau, H. M. (1990) Accelerated age-related decline in replicative life-span of Duchenne muscular dystrophy myoblasts: implications for cell and gene therapy. *Somat. Cell Mol. Genet.* **16,** 557–565
12. Hashimoto, N., Murase, T., Kondo, S., Okuda, A., and Inagawa-Ogashiwa, M. (2004) Muscle reconstitution by muscle satellite

cell descendants with stem cell-like properties. *Development (Camb.)* **131,** 5481–5490
13. Montarras, D., Morgan, J., Collins, C., Relaix, F., Zaffran, S., Cumano, A., Partridge, T., and Buckingham, M. (2005) Direct isolation of satellite cells for skeletal muscle regeneration. *Science* **309,** 2064–2067
14. Collins, C. A., Olsen, I., Zammit, P. S., Heslop, L., Petrie, A., Partridge, T. A., and Morgan, J. E. (2005) Stem cell function, self-renewal, and behavioral heterogeneity of cells from the adult muscle satellite cell niche. *Cell* **122,** 289–301
15. Partridge, T. A., Morgan, J. E., Coulton, G. R., Hoffman, E. P., and Kunkel, L. M. (1989) Conversion of mdx myofibres from dystrophin-negative to -positive by injection of normal myoblasts. *Nature* **337,** 176–179
16. Mendell, J. R., Kissel, J. T., Amato, A. A., King, W., Signore, L., Prior, T. W., Sahenk, Z., Benson, S., McAndrew, P. E., Rice, R., Nagaraja, H., Stephens, R., Lantry, L., Morris, G. E., and Burghes, A. H. M. (1995) Myoblast transfer in the treatment of Duchenne's muscular dystrophy. *N. Engl. J. Med.* **333,** 832–838
17. Weissman, I. L., Anderson, D. J., and Gage, F. (2001) Stem and progenitor cells: origins, phenotypes, lineage commitments, and transdifferentiations. *Annu. Rev. Cell Dev. Biol.* **17,** 387–403
18. Relaix, F., Montarras, D., Zaffran, S., Gayraud-Morel, B., Rocancourt, D., Tajbakhsh, S., Mansouri, A., Cumano, A., and Buckingham, M. (2006) Pax3 and Pax7 have distinct and overlapping functions in adult muscle progenitor cells. *J. Cell Biol.* **172,** 91–102
19. Seale, P., Sabourin, L. A., Girgis-Gabardo, A., Mansouri, A., Gruss, P., and Rudnicki, M. A. (2000) Pax7 is required for the specification of myogenic satellite cells. *Cell* **102,** 777–786
20. Cornelison, D. D., and Wold, B. J. (1997) Single-cell analysis of regulatory gene expression in quiescent and activated mouse skeletal muscle satellite cells. *Dev. Biol.* **191,** 270–283
21. Hollnagel, A., Grund, C., Franke, W. W., and Arnold, H. H. (2002) The cell adhesion molecule M-cadherin is not essential for muscle development and regeneration. *Mol. Cell. Biol.* **22,** 4760–4770
22. Bottaro, D. P., Rubin, J. S., Faletto, D. L., Chan, A. M., Kmiecik, T. E., Vande Woude, G. F., and Aaronson, S. A. (1991) Identification of the hepatocyte growth factor receptor as the c-met proto-oncogene product. *Science* **251,** 802–804
23. Fukada, S., Higuchi, S., Segawa, M., Koda, K., Yamamoto, Y., Tsujikawa, K., Kohama, Y., Uezumi, A., Imamura, M., Miyagoe-Suzuki, Y., Takeda, S., and Yamamoto, H. (2004) Purification and cell-surface marker characterization of quiescent satellite cells from murine skeletal muscle by a novel monoclonal antibody. *Exp. Cell Res.* **296,** 245–255
24. Dekel, I., Magal, Y., Pearson-White, S., Emerson, C. P., and Shani, M. (1992) Conditional conversion of ES cells to skeletal muscle by an exogenous MyoD1 gene. *New Biol.* **4,** 217–224
25. Rohwedel, J., Maltsev, V., Bober, E., Arnold, H. H., Hescheler, J., and Wobus, A. M. (1994) Muscle cell differentiation of embryonic stem cells reflects myogenesis in vivo: developmentally regulated expression of myogenic determination genes and functional expression of ionic currents. *Dev. Biol.* **164,** 87–101
26. Barberi, T., Bradbury, M., Dincer, Z., Panagiotakos, G., Socci, N. D., and Studer, L. (2007) Derivation of engraftable skeletal myoblasts from human embryonic stem cells. *Nat. Med.* **13,** 642–648
27. Doetschman, T. C., Eistetter, H., Katz, M., Schmidt, W., and Kemler, R. (1985) The in vitro development of blastocyst-derived embryonic stem cell lines: formation of visceral yolk sac, blood islands and myocardium. *J. Embryol. Exp. Morphol.* **87,** 27–45
28. Niwa, H., Yamamura, K., and Miyazaki, J. (1991) Efficient selection for high-expression transfectants with a novel eukaryotic vector. *Gene* **108,** 193–199
29. Yoshimoto, M., Chang, H., Shiota, M., Kobayashi, H., Umeda, K., Kawakami, A., Heike, T., and Nakahata, T. (2005) Two different roles of purified CD45+c-Kit+Sca-1+Lin-cells after transplantation in muscles. *Stem Cells (Dayton)* **23,** 610–618
30. Harris, J. B. (2003) Myotoxic phospholipases A2 and the regeneration of skeletal muscles. *Toxicon* **42,** 933–945
31. Fukada, S., Miyagoe-Suzuki, Y., Tsukihara, H., Yuasa, K., Higuchi, S., Ono, S., Tsujikawa, K., Takeda, S., and Yamamoto, H. (2002) Muscle regeneration by reconstitution with bone marrow or fetal liver cells from green fluorescent protein-gene transgenic mice. *J. Cell Sci.* **115,** 1285–1293
32. Gross, J. G., and Morgan, J. E. (1999) Muscle precursor cells injected into irradiated mdx mouse muscle persist after serial injury. *Muscle Nerve* **22,** 174–185
33. Rosenblatt, J. D., Lunt, A. I., Parry, D. J., and Partridge, T. A. (1995) Culturing satellite cells from living single muscle fiber explants. *In Vitro Cell. Dev. Biol.* **31,** 773–779
34. Dhawan, J., and Rando, T. A. (2005) Stem cells in postnatal myogenesis: molecular mechanisms of satellite cell quiescence, activation and replenishment. *Trends Cell Biol.* **15,** 666–673
35. Zammit, P. S., Relaix, F., Nagata, Y., Ruiz, A. P., Collins, C. A., Partridge, T. A., and Beauchamp, J. R. (2006) Pax7 and myogenic progression in skeletal muscle satellite cells. *J. Cell Sci.* **119,** 1824–1832
36. Relaix, F., Rocancourt, D., Mansouri, A., and Buckingham, M. (2005) A Pax3/Pax7-dependent population of skeletal muscle progenitor cells. *Nature* **435,** 948–953
37. Tajbakhsh, S., Rocancourt, D., Cossu, G., and Buckingham, M. (1997) Redefining the genetic hierarchies controlling skeletal myogenesis: Pax-3 and Myf-5 act upstream of MyoD. *Cell* **89,** 127–138
38. Kiefer, J. C., and Hauschka, S. D. (2001) Myf-5 is transiently expressed in nonmuscle mesoderm and exhibits dynamic regional changes within the presegmented mesoderm and somites I-IV. *Dev. Biol.* **232,** 77–90
39. Hirsinger, E., Malapert, P., Dubrulle, J., Delfini, M. C., Duprez, D., Henrique, D., Ish-Horowicz, D., and Pourquie, O. (2001) Notch signalling acts in postmitotic avian myogenic cells to control MyoD activation. *Development (Camb.)* **128,** 107–116
40. Smith, T. H., Block, N. E., Rhodes, S. J., Konieczny, S. F., and Miller, J. B. (1993) A unique pattern of expression of the four muscle regulatory factor proteins distinguishes somitic from embryonic, fetal and newborn mouse myogenic cells. *Development (Camb.)* **117,** 1125–1133
41. Kassar-Duchossoy, L., Giacone, E., Gayraud-Morel, B., Jory, A., Gomes, D., and Tajbakhsh, S. (2005) Pax3/Pax7 mark a novel population of primitive myogenic cells during development. *Genes Dev.* **19,** 1426–1431
42. Harrison, D. E., Astle, C. M., and Delaittre, J. A. (1978) Loss of proliferative capacity in immunohemopoietic stem cells caused by serial transplantation rather than aging. *J. Exp. Med.* **147,** 1526–1531
43. Yao, S. N., and Kurachi, K. (1993) Implanted myoblasts not only fuse with myofibers but also survive as muscle precursor cells. *J. Cell Sci.* **105**(Pt. 4), 957–963
44. Rando, T. A., and Blau, H. M. (1994) Primary mouse myoblast purification, characterization, and transplantation for cell-mediated gene therapy. *J. Cell Biol.* **125,** 1275–1287
45. Sherwood, R. I., Christensen, J. L., Conboy, I. M., Conboy, M. J., Rando, T. A., Weissman, I. L., and Wagers, A. J. (2004) Isolation of adult mouse myogenic progenitors: functional heterogeneity of cells within and engrafting skeletal muscle. *Cell* **119,** 543–554
46. Darabi, R., Gehlbach, K., Bachoo, R. M., Kamath, S., Osawa, M., Kamm, K. E., Kyba, M., and Perlingeiro, R. C. (2008) Functional skeletal muscle regeneration from differentiating embryonic stem cells. *Nat. Med.* **14,** 134–143

Received for publication October 21, 2008.
Accepted for publication January 8, 2009.

European Journal of Haematology ISSN 0902-4441

ORIGINAL ARTICLE

AKR-501 (YM477) a novel orally-active thrombopoietin receptor agonist

Mari Fukushima-Shintani[1*], Ken-ichi Suzuki[2*], Yoshiyuki Iwatsuki[2], Masaki Abe[2], Keizo Sugasawa[2], Fukushi Hirayama[2], Tomihisa Kawasaki[3], Tatsutoshi Nakahata[4]

[1]QA, RA and Pharmacovigilance, Astellas Pharma Inc., Itabashi-ku, Tokyo, Japan; [2]Drug Discovery Research, Astellas Pharma Inc., Tsukuba, Ibaraki, Japan; [3]Development, Astellas Pharma Inc., Itabashi-ku, Tokyo, Japan; [4]Department of Pediatrics, Kyoto University Graduate School of Medicine, Shogoin, Sakyo-ku, Kyoto, Japan

Abstract

Thrombopoietin (TPO) is the principal physiologic regulator of platelet production. We have searched for small molecule compounds that mimic the action of TPO by using human TPO receptor-expressed in Ba/F3 cells, resulting in the discovery of AKR-501 (YM477). AKR-501 specifically targeted the TPO receptor and stimulated megakaryocytopoiesis throughout the development and maturation of megakaryocytes just as rhTPO did. AKR-501, however, was shown to be effective only in humans and chimpanzees with high species specificity. Therefore, we examined the *in vivo* platelet-increasing effect of AKR-501 in human platelet producing non-obese diabetic/severe combined immunodeficiency (NOD/SCID) mice transplanted with human fetal liver $CD34^+$ cells. Daily oral administration of AKR-501 dose-dependently increased the number of human platelets in these mice, with significance achieved at doses of 1 mg/kg and above. The peak unbound plasma concentrations of AKR-501 after administration at 1 mg/kg in NOD/SCID mice were similar to those observed following administration of an active oral dose in human subjects. These results suggest that AKR-501 is an orally-active TPO receptor agonist that may be useful in the treatment of patients with thrombocytopenia.

Key words thrombopoietin; thrombopoiesis; c-mpl; platelets; NOD/SCID mice; AKR-501; YM477

Correspondence Ken-ichi Suzuki, PhD., Pharmacology Research Laboratories, Astellas Pharma Inc., 21 Miyukigaoka, Tsukuba, Ibaraki 305-8585, Japan. Tel: +81 29 852 5111; Fax: +81 29 852 2955; e-mail: kenichi-suzuki@jp.astellas.com

*Contributed equally to this work.

Accepted for publication 26 November 2008

doi:10.1111/j.1600-0609.2008.01198.x

While platelet development appears to be regulated by a number of growth factors and cytokines, thrombopoietin (TPO) is the principal physiologic regulator of platelet production (1, 2). TPO stimulates megakaryocytopoiesis throughout the development and maturation of megakaryocytes leading to platelet production. The TPO receptor is expressed on hematopoietic stem cells (HSCs), a subfraction of hematopoietic precursors, and on cells of the megakaryocytic lineage and platelets. Two TPO receptor agonists, recombinant human TPO (rhTPO) and pegylated recombinant megakaryocyte growth and development factor (PEG-rHuMGDF), have previously undergone extensive clinical trials. However, the clinical development of PEG-rHuMGDF was terminated because of the development of neutralizing antibodies to PEG-rHuMGDF that cross-reacted with endogenous thrombopoietin, resulting in profound hematological consequences in patients and volunteers receiving multiple subcutaneous injections of the drug (3, 4). The appearance of antibodies was reported in an early trial of rhTPO, but the biological activity of these antibodies has not been reported (5). Recombinant

TPOs are therefore associated with risk of immunogenicity.

Recently, a number of screening methods have been developed to identify small molecules that could mimic the biological effects of hematopoietic growth factors. Potential advantages of small molecule mimetics include their putative lack of immunogenicity and non-parenteral route of administration. Small molecules might also be less expensive to produce. To identify small molecule mimetics of native proteins, high throughput assays of either receptor binding or biological activity have been devised. With respect to TPO, several small molecular compounds were reported to mimic the effect of TPO through the TPO receptor (6–10). Therefore, we screened by using human TPO receptor transfected murine Ba/F3 cells to identify orally active small molecular TPO receptor agonists (11), which led to the discovery of AKR-501.

Here, we describe the pharmacological properties of AKR-501. We showed that AKR-501 mimics the biological activities of TPO *in vitro* and *in vivo*. AKR-501, however, was showed to have effect in humans and chimpanzees only. Non-obese diabetic/severe combined immunodeficiency (NOD/SCID) mice were characterized as representing an efficient engraftment model for human HSCs, which resulted in the production of human platelets. Therefore, this model was used in this study to examine the effect of AKR-501 on *in vivo* platelet production in human platelet producing NOD/SCID mice in which human HSCs has been transplanted. Further, we demonstrated that this model is suitable to predict the effect of AKR-501 in humans.

Materials and methods

Compounds

AKR-501, 1-(3-Chloro-5-{[4-(4-chloro-2-thienyl)-5-(4-cyclohexylpiperazin-1-yl)-1,3-thiazol-2-yl]carbamoyl}-2-pyridyl) piperidine-4-carboxylic acid was synthesized by Yamanouchi Pharmaceutical Co., Ltd. (Ibaraki, Japan) (12). rhTPO was purchased from GT (Minneapolis, MN, USA).

Human TPO receptor expressed Ba/F3 cells

The human full-length *c-mpl* cDNA (*c-mpl-p*) derived from HEL cells was subcloned into a pEF-BOS vector. This plasmid pEF-BOS-*c-mpl* (10 μg) and the selection marker plasmid pSV2bsr (1 μg) (Kaken-Seiyaku, Tokyo, Japan) were co-electroporated into murine IL-3 (mIL-3) dependent murine Ba/F3 cells in a 0.4 cm cuvette at 1.5 kV (25 μF). These cells were then cultured in RPMI 1640 medium (GIBCO, Grand Island, NY, USA) supplemented with WEHI conditioned media (BD Biosciences, Bedford, MA, USA) for 3 d, and then in selection medium containing 10 μg/mL blasticidin (Funakoshi, Tokyo, Japan) for 1 month.

Assay for TPO receptor-dependent cell growth

The cells used in this study were maintained in RPMI 1640 medium supplemented with 10% FBS (JRH BIOSCIENCES, Lenexa, KS, USA), 50 units/mL penicillin/streptomycin (GIBCO), and WEHI conditioned media. These cells were seeded in each well of a 96-well plate and cultured in the medium at the concentration of 2×10^5 cells/mL. Human TPO receptor expressing Ba/F3 cells were incubated with AKR-501, dissolved in dimethyl sulfoxide (DMSO), or rhTPO. Ba/F3 cells were incubated with AKR-501, rhTPO or recombinant mIL-3 (rmIL-3; Pepro Tech EC, London, UK). WST-1/1-methoxy PMS reagent (Cell counting kit, Dojin, Kumamoto, Japan) was added to each well and then incubated. A450/A655 was measured with a microplate reader (Model 3350; BioRad, Hercules, CA, USA) immediately and at 2 h after addition of WST-1/1-methoxy PMS reagent. Proliferation activity of the compound was calculated as the percentage of maximum proliferative activity of rhTPO for TPO receptor expressing Ba/F3 cells. The percentage of maximum proliferative activity of rmIL-3 was used to calculate the proliferation activity for Ba/F3 cells.

Megakaryocyte colony formation

Human cord blood (CB) $CD34^+$ cells (AllCells, Berkeley, CA, USA) at a density of 2500 cells/0.75 mL were suspended in MegaCult™-C (StemCell Technologies Inc., Vancouver, Canada) containing either AKR-501 dissolved in DMSO or rhTPO, and plated in two-well chamber slides. After 10–12 d of incubation, human CD41-positive megakaryocytes were identified. Colonies that contained three or more human CD41-positive cells were scored as human megakaryocyte colonies. Data were expressed as the percentage of maximum differentiation activity of rhTPO, and the EC_{50} values were calculated for the drug.

Ploidy analysis

G-CSF-mobilized human peripheral blood $CD34^+$ cells (BioWhittaker Inc., Walkersville, MD, USA) were seeded in a 24-well culture plate (Iwaki, Chiba, Japan) at 10 000 cells/0.5 mL/well in culture medium in the presence of 3 μM AKR-501 or 3 nM rhTPO. The culture medium consisted of 100 μM 2-mercaptoethanol, 7.5 μg/mL

cholesterol, BIT9500 (StemCell Technologies Inc.), and Iscove's modified Dulbecco's medium. The cells were cultured for 12 d at 37°C. The cells were collected and stained with anti-human CD41-FITC (BD PharMingen, San Diego, CA, USA). After incubation for 20 min at 4°C, cells were washed, made permeable by gradual addition of methanol which was chilled at −40°C, and incubated for 30 min at 4°C. Then, cells were treated with 100 μg/mL RNase (Nippon Gene, Toyama, Japan) for 30 min at 4°C, and 50 μg/mL propidium iodide (PI) (Sigma, St. Louis, MO, USA) was added. After incubation for 30 min under darkness at 4°C, the cells were suspended in 500 μL of 2% FBS-PBS and analyzed using a flow cytometry (EPICS XL-MCL, Beckman-Coulter, Miami, FL, USA). Cells expressing CD41 were regarded as megakaryocytes. Ploidy distribution was analyzed by histogram. Events of each peak were counted by setting markers. Each ploidy level was expressed as event %. Event % at ploidy level of nN was calculated by the followed equation; Events % (nN) = [nN/(2N + 4N + 8N + 16N + 32N<)] × 100.

Western blot analysis of signal transduction through TPO receptor

Human TPO receptor expressing Ba/F3 cells washed free of growth factors by media, were incubated in RPMI1640 supplemented with 10% FBS and 50 units/mL penicillin/streptomycin for 15 h at 37°C. After this depletion period, cells were resuspended in RPMI1640 at a concentration of 1×10^6/mL and were stimulated with either AKR-501 or rhTPO at 37°C for 15 min. Cells were lysed in the same volume of a buffer containing 15 mM HEPES (pH 7.4), 150 mM NaCl, 10 mM EGTA, 1 mM sodium orthovanadate, protease inhibitor cocktail tablet (Roche Diagnostics, Indianapolis, IN, USA), and 2% (w/v) Triton X-100. Insoluble materials were removed by centrifugation at 10 000 × *g* for 30 min at 4°C. Total lysates were separated by electrophoresis using an SDS-PAGE gel under reducing conditions and transferred to a sheet of polyvinylidene difluoride membrane (Millipore, Bedford, MA, USA). The membrane was then blocked with Block Ace (Dainihon-Seiyaku, Osaka, Japan) at room temperature for 30 min. Membranes were then incubated overnight at 4°C in a hybridization buffer consisting of anti-phospho-STAT3 (Tyr705), anti-phospho-STAT5 (Tyr694), and anti-phospho-ERK (Thr202, 204) antibodies (Cell Signaling, Beverly, MA, USA) in Tris-buffered saline with 0.05% Tween 20 (TBST), and 3% FBS. These filters were stripped and reprobed with anti-STAT3, anti-STAT5 (Santa Cruz Biotechnology, CA, USA), and anti-ERK antibodies (Upstate Biotechnology, Lake Placid, NY, USA) to assure equal loading in each lane of the gel. Blots were developed using an ECL kit (Amersham Pharmacia, Buckinghamshire, UK).

Western blot analysis of tyrosine phosphorylation of STAT 5 in the platelets

Human blood was drawn from healthy volunteers in the presence of a 1/10th volume of 3.8% sodium citrate, added as an anticoagulant, and centrifuged at 150 × *g* for 10 min to obtain platelet-rich plasma (PRP). Animal blood from various species (chimpanzee, olive baboon, rhesus monkey, cynomolgus monkey, common marmoset, squirrel monkey, beagle dog, guinea pig, rabbit, rat, and hamster) were drawn in the presence of 1/10th volume of 3.8% sodium citrate. PRP was prepared by centrifugation of whole blood at 170 × *g* for 10 min. After the addition of 5 nM PGE_1 (Sigma), 5 mM EDTA (pH 8.05), and 3 U/mL apyrase (Sigma), the PRP was centrifuged at 1490 × *g* to form a platelet pellet. The pellet was resuspended in 5 mL of a Tyrode's-HEPES buffer (137 mM NaCl, 2.68 mM KCl, 3.75 mM NaH_2PO_4, 0.98 mM $MgCl_2$, 5.55 mM dextrose, 0.35% (w/v) BSA, and 37.8 mM HEPES, pH 6.7) also containing 5 nM PGE_1, 5 mM EDTA (pH 8.05), and 3 U/mL apyrase and washed once. For western blot analysis, platelets were resuspended at a concentration of 3×10^8 cells/mL in the Tyrode's-HEPES buffer (pH 7.35) and were stimulated with either AKR-501 or rhTPO at 37°C for 15 min. The Western blot protocol was as described above. In the incubation process, membranes were in a hybridization buffer consisting of anti-phospho-STAT5 antibody in TBST and 3% FBS.

Transplantation of human fetal liver CD34$^+$ cells into NOD/SCID mice

Human fetal liver (FL) CD34$^+$ cells (approximately 1 00 000 cells/mouse, BioWhittaker Inc, Walkersville, MD, USA) were injected into 9- to 12-wk-old NOD/SCID mice through the tail vein after irradiation with 2.4 Gy as two divided doses at intervals of at least 4 h by an X-ray apparatus (MBR-1520R-3, Hitachi Medical Corporation, Tokyo, Japan). The transplanted mice were injected intraperitoneally with anti-asialo GM1 antiserum (Wako, Osaka, Japan) immediately before cell transplantation and every 9–11 d after cell transplantation, a total of six times in order to deplete natural killer cells. After transplantation, mice were given sterile water containing prophylactic neomycin. Peripheral blood (PB) was obtained from the retro-orbital plexus using heparinized calibrated pipets (Drummond Scientific Co, Broomall, PA, USA), and transferred to EDTA 2Na containing Capiject (Terumo Medical, Somerset, NJ, USA). Blood cell counts were measured

using an automatic cell counter (MEK-6258, Nihon Kohden, Tokyo, Japan).

Flow cytometric analysis of peripheral blood in transplanted NOD/SCID mice

Human platelets from NOD/SCID mice were analyzed by flow cytometry (EPICS XL-MCL). Human platelets in PB were measured by staining with anti-human CD41-PE and anti-murine CD41-FITC (BD PharMingen). The percentage of human platelets was calculated by dividing the number of $hCD41^+$ cells by the total number of $CD41^+$ cells (human and mouse). The number of human platelets in PB was calculated by multiplying the percentage of human platelets by the total blood platelet count in PB, as measured with an automatic cell counter. The number of murine platelets in PB was calculated by subtracting the number of human platelets from the total platelet count.

Administration of AKR-501 to transplanted NOD/SCID mice

Various doses of AKR-501 (0, 0.3, 1, and 3 mg/kg/d), suspended in 0.5% methylcellulose, were orally administered for 14 d to NOD/SCID mice transplanted with human FL $CD34^+$ cells. PB was collected on days 7, 14, 21, and 28 after the start of AKR-501 administration, and blood cell counts and the number of human platelets were measured. The time course of changes in human and murine platelets number is expressed in terms of the rate of increase after administration of AKR-501 relative to the value at predosing. Statistical analysis was performed by Dunnett's test.

Results

AKR-501 is a TPO receptor agonist

We screened for small molecule compounds that mimic the action of TPO using a method that measured the proliferative activity of human TPO receptor-expressing Ba/F3 cells, resulting in the discovery of an orally active TPO receptor agonist, AKR-501. AKR-501 supported the proliferation of TPO receptor expressing Ba/F3 cell in a concentration-dependent fashion (Fig. 1A). The compound demonstrated an EC_{50} value of 3.3 ± 0.2 nM in this assay with the maximum proliferative activity equivalent to maximum activity of rhTPO. The activity of the compound was dependent on the TPO receptor, because parental Ba/F3 cells did not respond to either AKR-501 or rhTPO (Fig. 1A, B). Further, AKR-501 induced tyrosine phosphorylation of STAT3 and STAT5, and threonine phosphorylation of ERK in the cells, as

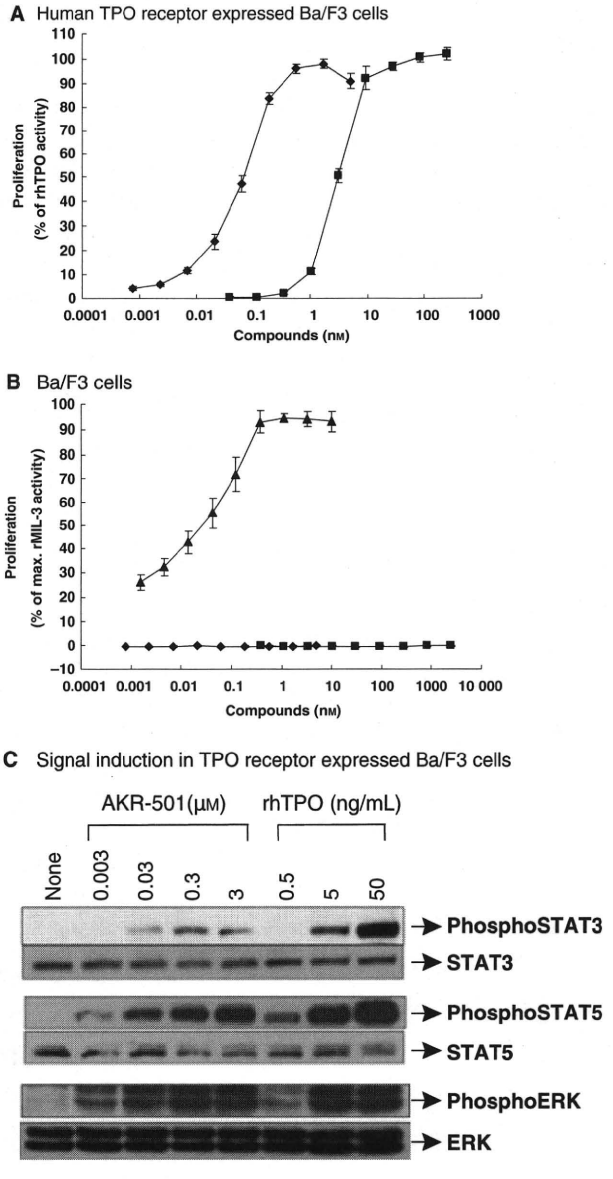

Figure 1 AKR-501 specifically acts on human Thrombopoietin (TPO) receptor. (A, B) Proliferative response of human TPO receptor expressed Ba/F3 cells (A) and Ba/F3 cells (B) to AKR-501 (■), rhTPO (♦), and rmIL-3 (▲). Data are presented as mean ± SE (n = 5). (C) Signal induction in TPO receptor expressed Ba/F3 cells. Human TPO receptor expressed Ba/F3 cells were stimulated by AKR-501 or rhTPO. Immunoblots were probed with anti-phospho-STAT3, anti-phospho-STAT5, and anti-phospho-ERK antibodies. These filters were stripped and reprobed with anti-STAT3, anti-STAT5, and anti-ERK antibodies.

did rhTPO. Thus, AKR-501 activates signal transduction in TPO receptor expressing Ba/F3 cells through the TPO receptor, and supports the proliferation of these cells (Fig. 1C).

TPO specifically stimulates megakaryocytopoiesis throughout the development and maturation of

megakaryocytes. Therefore, we examined the effect of AKR-501 on the differentiation to megakaryocytes from hematopoietic progenitor cells. AKR-501 promoted megakaryocyte colony formation from human CB $CD34^+$ cells in a concentration-dependent fashion (Fig. 2A). The EC_{50} value was 25.0 ± 7.8 nM for AKR-501 and the maximum activity of AKR-501 was similar to that of rhTPO. Human megakaryocyte colonies generated with AKR-501 and rhTPO had similar morphologic features (Fig. 2B, C). Further, AKR-501 and rhTPO induced polyploidization of megakaryocytes from G-CSF mobilized peripheral blood $CD34^+$ cells in liquid culture (Fig. 3A, B). There was no apparent difference between AKR-501 and rhTPO at each ploidy level (Fig. 3C). These results suggest that AKR-501 mimics the effect of TPO *in vitro*.

Species specificity of AKR-501

TPO receptor is expressed on the surface of platelets, and TPO induces signal transduction including STAT5. The species specificity of AKR-501 for the TPO receptor was demonstrated by STAT5 activation in platelets of various species (Fig. 4). AKR-501 induced tyrosine phosphorylation of STAT5 in human blood platelets and chimpanzee blood platelets, as did rhTPO. In contrast, rhTPO induced tyrosine phosphorylation of STAT5 in olive baboon, cynomolgus monkey, rhesus monkey, common marmoset, squirrel monkey, beagle dog, guinea pig, rabbit, rat, and hamster platelets (data not shown), but AKR-501 did not induce phosphorylation in these species.

Evaluation of AKR-501 on human platelet production in NOD/SCID mice

AKR-501 was shown to have strict species-specificity and to be effective only in humans and chimpanzees. To examine the *in vivo* pharmacological effects of AKR-501 on human platelet production, we used NOD/SCID mice transplanted with FL $CD34^+$ cells. NOD/SCID mice were characterized as an efficient engraftment model for HSCs. It had been reported that the multilineages of human hematopoiesis, including the production of human platelets, could be reconstituted over a long period of time in NOD/SCID mice transplanted with human HSCs (13, 14). In this study, we used commercially available cryopreserved human FL $CD34^+$ cells as a source of HSCs.

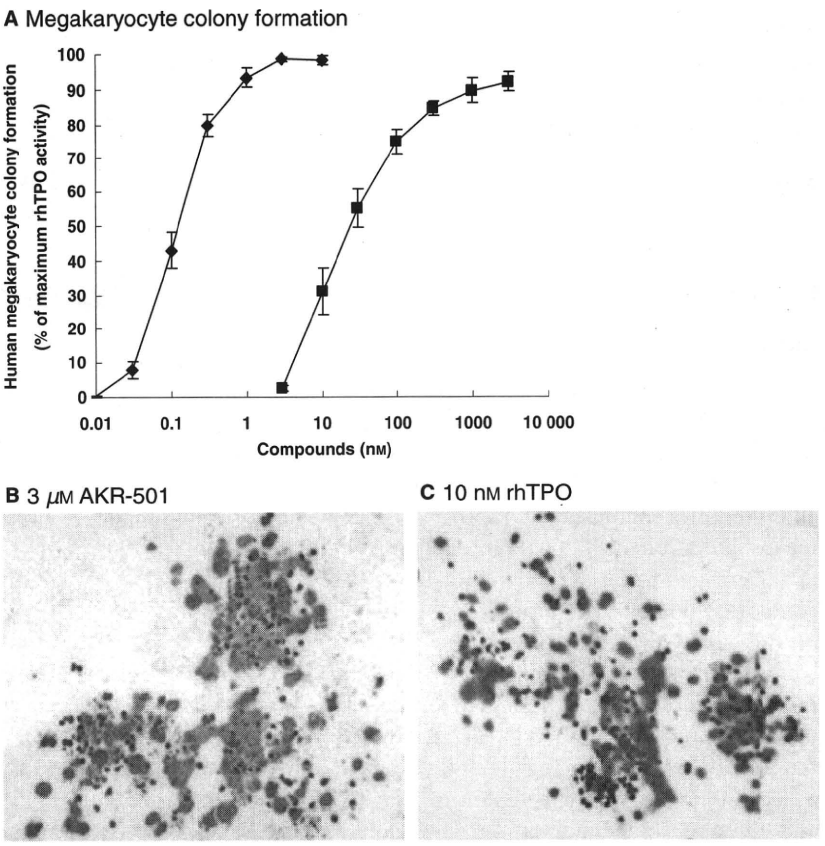

Figure 2 AKR-501 promotes megakaryocyte differentiation from human $CD34^+$ cells. (A) Megakaryocyte colony formation was measured in serum-free collagen-based medium cultures of human cord blood $CD34^+$ cells in the presence of increasing concentrations of AKR-501 (■), and recombinant human TPO (rhTPO) (♦). Data are presented as mean ± SE (n = 5). (B, C) Immunohistochemical identification of typical human megakaryocyte colonies generated with 3 μM AKR-501 (B) and 10 nM rhTPO (C) × 100 objectives.

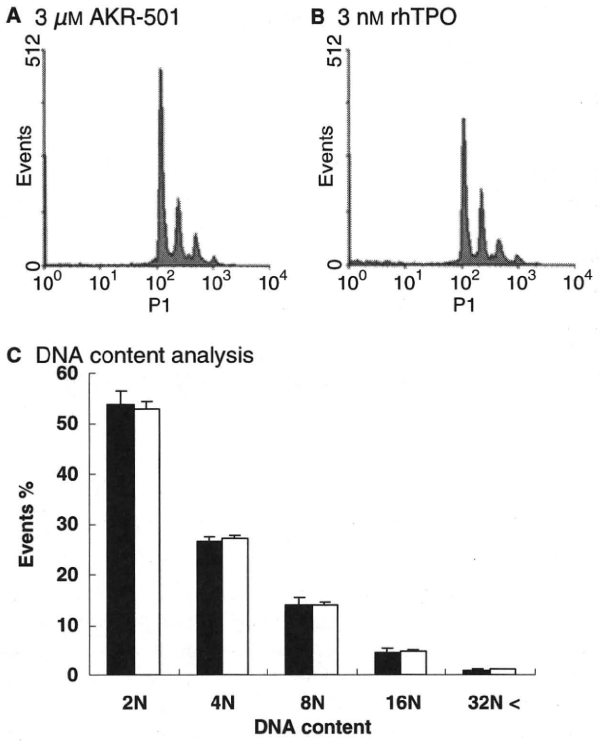

Figure 3 AKR-501 induces polyploidization of megakaryocytes. G-CSF-mobilized human peripheral blood $CD34^+$ cells were cultured for 12 d in serum-free liquid medium in the presence of 3 μM AKR-501 or 3 nM recombinant human TPO (rhTPO). Following surface marker staining, DNA analysis was performed by staining with propidium iodide. The plots show the typical ploidy distribution after gating on $CD41^+$ cells (A: 3 μM AKR-501, B: 3 nM rhTPO). (C) Ploidy analysis of megakaryocytes generated by 3 μM AKR-501 (open columns) or 3 nM rhTPO (filled columns). The data represent the mean ± SE of five independent experiments. Statistical analysis was performed in each DNA content group using Student's *t*-test.

Human platelets started to appear in the PB of these mice 4 wk after transplantation. The production of human platelets continued for more than 6 months post-transplant.

Doses of 0.3, 1, and 3 mg/kg/d of AKR-501 were orally administered once per day for 14 d to NOD/SCID mice that stably produced human platelets. Oral administration of AKR-501 dose-dependently increased the number of human platelets, resulting in approximately a 2.7-fold increase at 1 mg/kg/d ($P < 0.05$) and a 3.0-fold increase ($P < 0.01$) at 3 mg/kg/d on day 14 after the start of administration (Fig. 5A). The minimum effective dose was 1 mg/kg/d. Withdrawal of AKR-501 administration caused the human platelet count to return nearly to pretreatment levels. As was expected given the species selective activity of AKR-501, the murine platelet count did not change after oral administration of AKR-501 at any dosage (Fig. 5B). Further, WBC, RBC, and body weight did not significantly change during the study period (data not shown).

Discussion

We successfully employed high throughput screening techniques based on proliferation of human TPO receptor-expressing Ba/F3 cells to identify a series of 2-acylaminothiazole derivatives as a potent novel series of TPO receptor agonists. The lead agent in the series, AKR-501, caused dose-dependent proliferation of human TPO receptor-expressing Ba/F3 cells and promoted differentiation to human megakaryocytes. This agent was efficacious following oral administration, producing a dose-dependent increase of human platelet numbers in NOD/SCID mice transplanted with human FL $CD34^+$ cells.

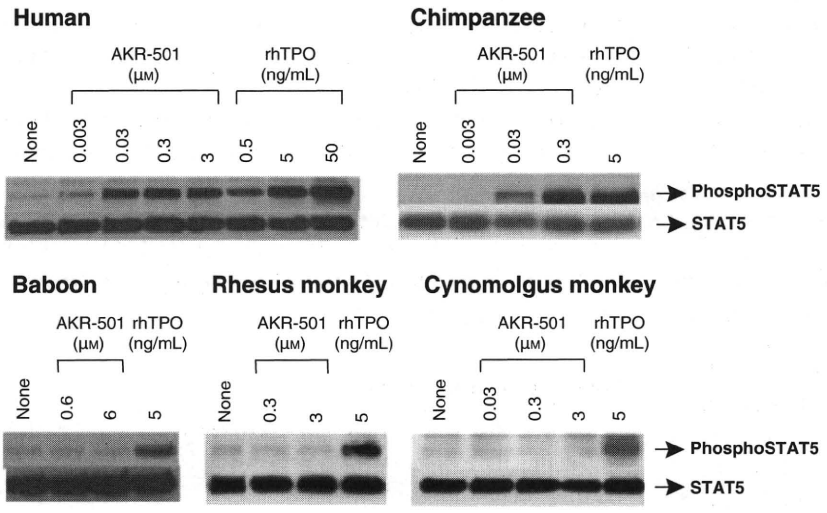

Figure 4 AKR-501 activates STAT5 in human and chimpanzee platelets, but not in baboon, rhesus, and cynomolgus monkey platelets. Human and non-human primate platelets were stimulated by AKR-501 or recombinant human TPO (rhTPO). Immunoblots were probed with anti-phospho-STAT5 antibody. These filters were stripped and reprobed with anti-STAT5 antibody.

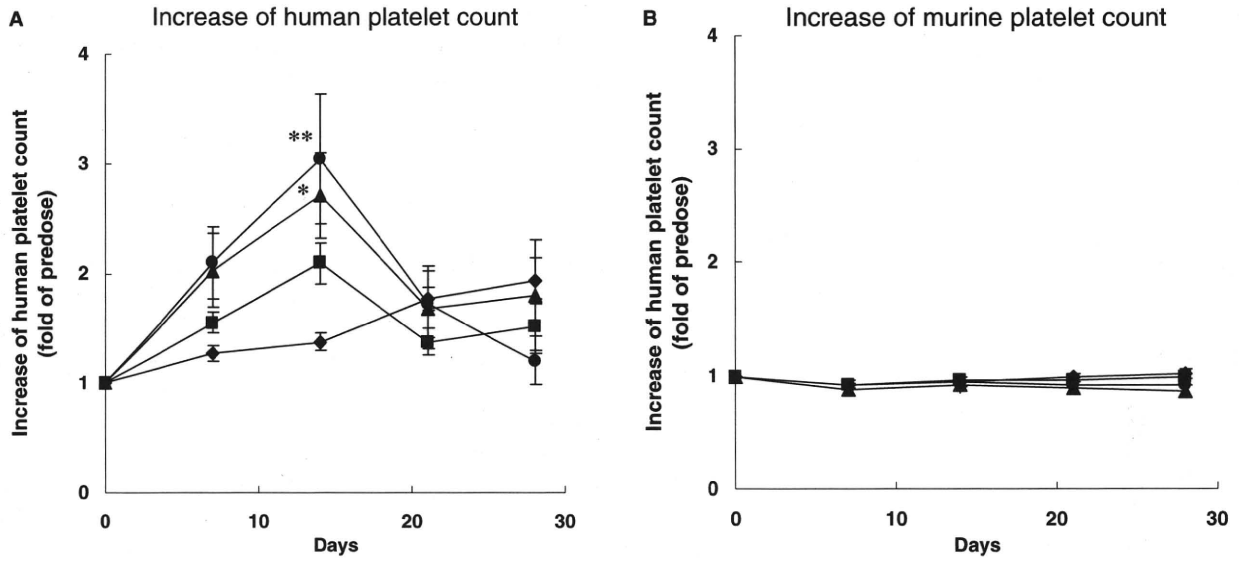

Figure 5 Oral administration of AKR-501 increases the number of human platelets in NOD/SCID mice transplanted with human FL CD34$^+$ cells. AKR-501 (vehicle (♦), 0.3 (■), 1 (▲), and 3 (•) mg/kg/d) was orally administered for 14 d to human platelet-producing NOD/SCID mice. PB was collected on the indicated days, and blood cell counts were measured. The percentage of human platelets was measured by flow cytometry, and the number of human (A) and murine platelets (B) was calculated as described in 'Materials and methods'. The time course of changes in human and murine platelet count is expressed in terms of the fold increase after administration of AKR-501 relative to the value at predosing. Data are presented as mean ± SE (n = 10, on day 28; n = 9 for vehicle, 0.3, 3 mg/kg/d groups). *$P < 0.05$, **$P < 0.01$ vs. vehicle group by Dunnett's test.

Other small molecules such as TM41 (15), SB-497115 (eltrombopag) (16), SB-394725 (17), and NIP-004 (18) have been reported as TPO receptor agonists. Some compounds including eltrombopag, SB-394725, and NIP-004 display species specificities (17–19) as did the compounds in our series. In order to identify an orally active TPO receptor agonist, we utilized NOD/SCID mice transplanted with human FL CD34$^+$ cells to evaluate hematopoietic stem cells (20–22) and human platelet production (13, 14). Previously we reported that subcutaneous injection of TPO to NOD/SCID mice transplanted with human cord blood CD34$^+$ cells dose-dependently increased the number of human platelets (14), and subcutaneous injection of NIP-004 has been shown to induce human platelet production in a xenotransplatation model (18). Herein we report that oral administration of AKR-501 to the NOD/SCID mice model increased the number of human platelets. To our knowledge, no other TPO agonists have been reported to be orally administered to the NOD/SCID mice model. Therefore, AKR-501 is the first TPO receptor agonist whose platelet increasing effect was proven by oral administration to NOD/SCID mice transplanted with human hematopoietic stem cells.

The efficacy of AKR-501 seen in the non-clinical model has also been demonstrated in the clinic. In a phase I study, once daily oral administration of AKR-501 at 10 mg to healthy volunteers for 14 d increased the number of platelets, resulting in a > 50% increase over baseline platelet count (23). This result is consistent with the *in vivo* result using NOD/SCID mice transplanted with human FL CD34$^+$ cells. Furthermore, similar peak unbound plasma concentrations of AKR-501 were observed in both the non-clinical model and in this phase I clinical trial. The peak unbound plasma concentrations of AKR-501 after administration at 1 mg/kg in the NOD/SCID mice study and after 14 d dosing at 10 mg/d in human study were 3.3 and 3.4 ng/mL, respectively. The observed pharmacodynamic responses at comparable exposures demonstrate that the NOD/SCID model is suitable for predicting the concentration-effect relationship of orally-active TPO receptor agonists in man.

In conclusion, we identified a novel orally-active TPO receptor agonist, AKR-501, which mimics the biological activity of TPO both *in vitro* and *in vivo*. These non-clinical results and early results from clinical investigations suggest that AKR-501 is an orally active TPO receptor agonist that may prove useful for treating patients with thrombocytopenia.

Acknowledgements

We gratefully acknowledge Dr. Robert E. Desjardins for reviewing the manuscript and Dr. Stephen J. Waters for editing the manuscript.

Authorship

Contribution: M.F-S. performed research, analyzed data, and wrote the paper, K.Suzuki designed research, performed research, analyzed data and edited the paper, Y.I., M.A. and K.Sugasawa performed research, F.H. analyzed data, T.K. analyzed data and edited the paper, and T.N supervised the study.

Conflict-of-interest disclosure

Tatsutoshi Nakahata declares no competing financial interests. Other authors are employees of Astellas Pharma Inc.

References

1. Kaushansky K. Thrombopoietin. *N Engl J Med* 1998;**339**:746–54.
2. Kaushansky K, Drachman JG. The molecular and cellular biology of thrombopoietin: the primary regulator of platelet production. *Oncogene* 2002;**21**:3359–67.
3. Li J, Yang C, Xia Y, Bertino A, Glaspy J, Roberts M, Kuter DJ. Thrombocytopenia caused by the development of antibodies to thrombopoietin. *Blood* 2001;**98**:3241–8.
4. Basser RL, O'Flaherty E, Green M, Edmonds M, Nichol J, Menchaca DM, Cohen B, Begley CG. Development of pancytopenia with neutralizing antibodies to thrombopoietin after multicycle chemotherapy supported by megakaryocyte growth and development factor. *Blood* 2002;**99**:2599–602.
5. Vadhan-Raj S, Murray LJ, Bueso-Ramos C, *et al.* Stimulation of megakaryocyte and platelet production by a single dose of recombinant human thrombopoietin in patients with cancer. *Ann Intern Med* 1997;**126**:673–81.
6. Kuter DJ. New thrombopoietic growth factors. *Blood* 2007;**109**:4607–16.
7. Reiter LA, Subramanyam C, Mangual EJ, *et al.* Pyrimidine benzamide-based thrombopoietin receptor agonists. *Bioorg Med Chem Lett* 2007;**17**:5447–54.
8. Alper PB, Marsilje TH, Mutnick D, *et al.* Discovery and biological evaluation of benzo[a]carbazole-based small molecule agonists of the thrombopoietin (Tpo) receptor. *Bioorg Med Chem Lett* 2008;**18**: 5255–8.
9. Marsilje TH, Alper PB, Lu W, *et al.* Optimization of small molecule agonists of the thrombopoietin (Tpo) receptor derived from a benzo[a]carbazole hit scaffold. *Bioorg Med Chem Lett* 2008;**18**:5259–62.
10. Reiter LA, Jones CS, Brissette WH, *et al.* Molecular features crucial to the activity of pyrimidine benzamide-based thrombopoietin receptor agonists. *Bioorg Med Chem Lett* 2008;**18**:3000–6.
11. Duffy KJ, Darcy MG, Delorme E, *et al.* Hydrazinonaphthalene and azonaphthalene thrombopoietin mimics are nonpeptidyl promoters of megakaryocytopoiesis. *J Med Chem* 2001;**44**:3730–45.
12. Fukushima-Shintani M, Suzuki K, Iwatsuki Y, Abe M, Sugasawa K, Hirayama F, Kawasaki T. AKR-501 (YM477) in combination with thrombopoietin enhances human megakaryocytopoiesis. *Exp Hematol* 2008;**36**:1337–42.
13. Ueda T, Yoshino H, Kobayashi K, Kawahata M, Ebihara Y, Ito M, Asano S, Nakahata T, Tsuji K. Hematopoietic repopulating ability of cord blood CD34(+) cells in NOD/Shi-scid mice. *Stem Cells* 2000;**18**:204–13.
14. Suzuki K, Hiramatsu H, Fukushima-Shintani M, Heike T, Nakahata T. Efficient assay for evaluating human thrombopoiesis using NOD/SCID mice transplanted with cord blood $CD34^+$ cells. *Eur J Haematol* 2007;**78**:123–30.
15. Kimura T, Kaburaki H, Tsujino T, Ikeda Y, Kato H, Watanabe Y. A non-peptide compound which can mimic the effect of thrombopoietin via c-Mpl. *FEBS Lett* 1998;**428**:250–4.
16. Erickson-Miller C, Delorme E, Giampa L, *et al.* Biological Activity and Selectivity for Tpo Receptor of the Orally Bioavailable, Small Molecule Tpo Receptor Agonist, SB-497115. *Blood (ASH Annual Meeting Abstracts)* 2004;**104**:2912.
17. Erickson-Miller CL, DeLorme E, Tian SS, *et al.* Discovery and characterization of a selective, nonpeptidyl thrombopoietin receptor agonist. *Exp Hematol* 2005;**33**:85–93.
18. Nakamura T, Miyakawa Y, Miyamura A, Yamane A, Suzuki H, Ito M, Ohnishi Y, Ishiwata N, Ikeda Y, Tsuruzoe N. A novel nonpeptidyl human c-Mpl activator stimulates human megakaryopoiesis and thrombopoiesis. *Blood* 2006;**107**:4300–7.
19. Erickson-Miller CL, Delorme E, Iskander M, *et al.* Species Specificity and Receptor Domain Interaction of a Small Molecule TPO Receptor Agonist. *Blood (ASH Annual Meeting Abstracts)* 2004;**104**:2909.
20. Dick JE, Bhatia M, Gan O, Kapp U, Wang JC. Assay of human stem cells by repopulation of NOD/SCID mice. *Stem Cells* 1997;**15**:199–203.
21. Greiner DL, Hesselton RA, Shultz LD. SCID mouse models of human stem cell engraftment. *Stem Cells* 1998;**16**:166–77.
22. Dao MA, Nolta JA. Immunodeficient mice as models of human hematopoietic stem cell engraftment. *Curr Opin Immunol* 1999;**11**:532–7.
23. Desjardins RE, Tempel DL, Lucek R, Kuter DJ. Single and multiple oral doses of AKR-501 (YM477) increase the platelet count in healthy volunteers. *ASH Annual Meeting Abstracts* 2006;**108**:477.

LETTERS

Frequent inactivation of A20 in B-cell lymphomas

Motohiro Kato[1,2], Masashi Sanada[1,5], Itaru Kato[6], Yasuharu Sato[7], Junko Takita[1,2,3], Kengo Takeuchi[8], Akira Niwa[6], Yuyan Chen[1,2], Kumi Nakazaki[1,4,5], Junko Nomoto[9], Yoshitaka Asakura[9], Satsuki Muto[1], Azusa Tamura[1], Mitsuru Iio[1], Yoshiki Akatsuka[11], Yasuhide Hayashi[12], Hiraku Mori[13], Takashi Igarashi[2], Mineo Kurokawa[4], Shigeru Chiba[3], Shigeo Mori[14], Yuichi Ishikawa[8], Koji Okamoto[10], Kensei Tobinai[9], Hitoshi Nakagama[10], Tatsutoshi Nakahata[6], Tadashi Yoshino[7], Yukio Kobayashi[9] & Seishi Ogawa[1,5]

A20 is a negative regulator of the NF-κB pathway and was initially identified as being rapidly induced after tumour-necrosis factor-α stimulation[1]. It has a pivotal role in regulation of the immune response and prevents excessive activation of NF-κB in response to a variety of external stimuli[2–7]; recent genetic studies have disclosed putative associations of polymorphic *A20* (also called *TNFAIP3*) alleles with autoimmune disease risk[8,9]. However, the involvement of A20 in the development of human cancers is unknown. Here we show, using a genome-wide analysis of genetic lesions in 238 B-cell lymphomas, that *A20* is a common genetic target in B-lineage lymphomas. A20 is frequently inactivated by somatic mutations and/or deletions in mucosa-associated tissue lymphoma (18 out of 87; 21.8%) and Hodgkin's lymphoma of nodular sclerosis histology (5 out of 15; 33.3%), and, to a lesser extent, in other B-lineage lymphomas. When re-expressed in a lymphoma-derived cell line with no functional *A20* alleles, wild-type A20, but not mutant A20, resulted in suppression of cell growth and induction of apoptosis, accompanied by downregulation of NF-κB activation. The A20-deficient cells stably generated tumours in immunodeficient mice, whereas the tumorigenicity was effectively suppressed by re-expression of A20. In A20-deficient cells, suppression of both cell growth and NF-κB activity due to re-expression of A20 depended, at least partly, on cell-surface-receptor signalling, including the tumour-necrosis factor receptor. Considering the physiological function of A20 in the negative modulation of NF-κB activation induced by multiple upstream stimuli, our findings indicate that uncontrolled signalling of NF-κB caused by loss of A20 function is involved in the pathogenesis of subsets of B-lineage lymphomas.

Malignant lymphomas of B-cell lineages are mature lymphoid neoplasms that arise from various lymphoid tissues[10,11]. To obtain a comprehensive registry of genetic lesions in B-lineage lymphomas, we performed a single nucleotide polymorphism (SNP) array analysis of 238 primary B-cell lymphoma specimens of different histologies, including 64 samples of diffuse large B-cell lymphomas (DLBCLs), 52 follicular lymphomas, 35 mantle cell lymphomas (MCLs), and 87 mucosa-associated tissue (MALT) lymphomas (Supplementary Table 1). Three Hodgkin's-lymphoma-derived cell lines were also analysed. Interrogating more than 250,000 SNP sites, this platform permitted the identification of copy number changes at an average resolution of less than 12 kilobases (kb). The use of large numbers of SNP-specific probes is a unique feature of this platform, and combined with the CNAG/AsCNAR software, enabled accurate determination of 'allele-specific' copy numbers, and thus allowed for sensitive detection of loss of heterozygosity (LOH) even without apparent copy-number reduction, in the presence of up to 70–80% normal cell contamination[12,13].

Lymphoma genomes underwent a wide range of genetic changes, including numerical chromosomal abnormalities and segmental gains and losses of chromosomal material (Supplementary Fig. 1), as well as copy-number-neutral LOH, or uniparental disomy (Supplementary Fig. 2). Each histology type had a unique genomic signature, indicating a distinctive underlying molecular pathogenesis for different histology types (Fig. 1a and Supplementary Fig. 3). On the basis of the genomic signatures, the initial pathological diagnosis of MCL was re-evaluated and corrected to DLBCL in two cases. Although most copy number changes involved large chromosomal segments, a number of regions showed focal gains and deletions, accelerating identification of their candidate gene targets. After excluding known copy number variations, we identified 46 loci showing focal gains (19 loci) or deletions (27 loci) (Supplementary Tables 2 and 3 and Supplementary Fig. 4).

Genetic lesions on the NF-κB pathway were common in B-cell lymphomas and found in approximately 40% of the cases (Supplementary Table 1), underpinning the importance of aberrant NF-κB activation in lymphomagenesis[11,14] in a genome-wide fashion. They included focal gain/amplification at the *REL* locus (16.4%) (Fig. 1b) and *TRAF6* locus (5.9%), as well as focal deletions at the *PTEN* locus (5.5%) (Supplementary Figs 1 and 4). However, the most striking finding was the common deletion at 6q23.3 involving a 143-kb segment. It exclusively contained the *A20* gene (also called *TNFAIP3*), a negative regulator of NF-κB activation[3–7,15] (Fig. 1b), which was previously reported as a candidate target of 6q23 deletions in ocular lymphoma[16]. LOH involving the *A20* locus was found in 50 cases, of which 12 showed homozygous deletions as determined by the loss of both alleles in an allele-specific copy number analysis (Fig. 1b, Table 1 and Supplementary Table 4). On the basis of this finding, we searched for possible tumour-specific mutations of *A20* by genomic DNA sequencing of entire coding exons of the gene in the same series of lymphoma samples (Supplementary Fig. 5). Because two out of the three Hodgkin's-lymphoma-derived cell lines had biallelic *A20* deletions/mutations (Supplementary Fig. 6), 24 primary samples from Hodgkin's lymphoma were also analysed for mutations, where

[1]Cancer Genomics Project, Department of [2]Pediatrics, [3]Cell Therapy and Transplantation Medicine, and [4]Hematology and Oncology, Graduate School of Medicine, University of Tokyo, 7-3-1 Hongo, Bunkyo-ku, Tokyo 113-8655, Japan. [5]Core Research for Evolutional Science and Technology, Japan Science and Technology Agency, 4-1-8, Honcho, Kawaguchi-shi, Saitama 332-0012, Japan. [6]Department of Pediatrics, Graduate School of Medicine, Kyoto University, 54 Kawahara-cho, Shogoin, Sakyo-ku, Kyoto 606-8507, Japan. [7]Department of Pathology, Okayama University Graduate School of Medicine, Dentistry and Pharmaceutical Sciences, 2-5-1 Shikata-cho, Kita-ku, Okayama 700-8558, Japan. [8]Division of Pathology, The Cancer Institute of Japanese Foundation for Cancer Research, Japan, 3-10-6 Ariake, Koto-ku, Tokyo 135-8550, Japan. [9]Hematology Division, Hospital, and [10]Early Oncogenesis Research Project, Research Institute, National Cancer Center, 5-1-1 Tsukiji, Chuo-ku, Tokyo 104-0045, Japan. [11]Division of Immunology, Aichi Cancer Center Research Institute, 1-1 Kanokoden, Chikusa-ku, Nagoya 464-8681, Japan. [12]Gunma Children's Medical Center, 779 Shimohakoda, Hokkitsu-machi, Shibukawa 377-8577, Japan. [13]Division of Hematology, Internal Medicine, Showa University Fujigaoka Hospital, 1-30, Fujigaoka, Aoba-ku, Yokohama-shi, Kanagawa 227-8501, Japan. [14]Department of Pathology, Teikyo University School of Medicine, 2-11-1 Kaga, Itabashi-ku, Tokyo 173-8605, Japan.

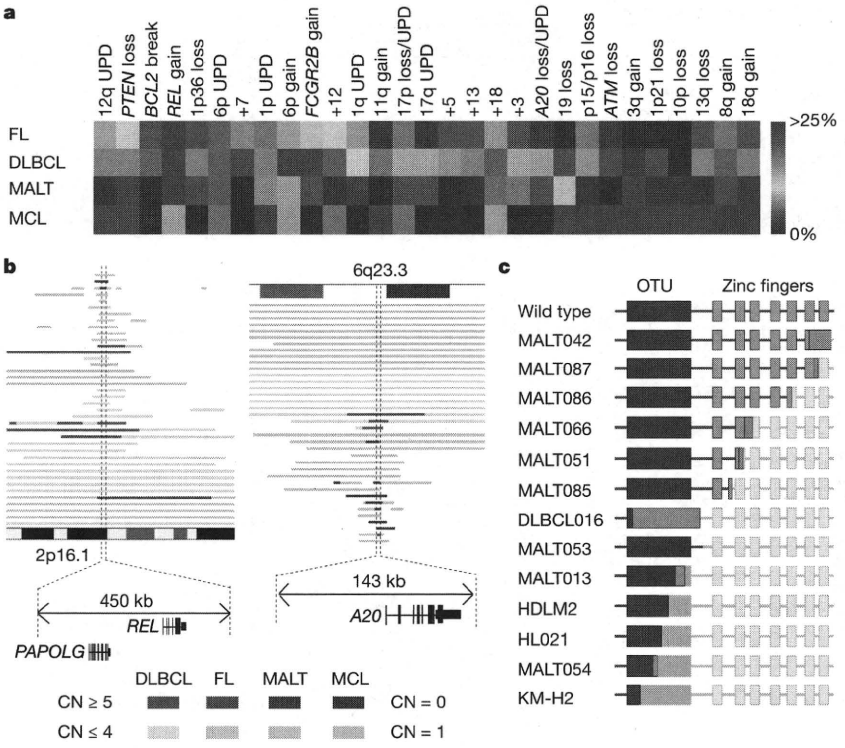

Figure 1 | Genomic signatures of different B-cell lymphomas and common genetic lesions at 2p16-15 and 6q23.3 involving NF-κB pathway genes. **a**, Twenty-nine genetic lesions were found in more than 10% in at least one histology and used for clustering four distinct histology types of B-lineage lymphomas. The frequency of each genetic lesion in each histology type is colour-coded. FL, follicular lymphoma; UPD, uniparental disomy. **b**, Recurrent genetic changes are depicted based on CNAG output of the SNP array analysis of 238 B-lineage lymphoma samples, which include gains at the *REL* locus on 2p16-15 (left panel) and the *A20* locus on 6q23.3 (right panel). Regions showing copy number gain or loss are indicated by horizontal lines. Four histology types are indicated by different colours, where high-grade amplifications and homozygous deletions are shown by darker shades to discriminate from simple gains (copy number ≤4) and losses (copy number = 1) (lighter shades). **c**, Point mutations and small nucleotide insertions and deletions in the *A20* (*TNFAIP3*) gene caused premature truncation of A20 in most cases. Altered amino acids caused by frame shifts are indicated by green bars.

genomic DNA was extracted from 150 microdissected CD30-positive tumour cells (Reed–Sternberg cells) for each sample. *A20* mutations were found in 18 out of 265 lymphoma samples (6.8%) (Table 1), among which 13 mutations, including nonsense mutations (3 cases), frame-shift insertions/deletions (9 cases), and a splicing donor site mutation (1 case) were thought to result in premature termination of translation (Fig. 1c). Four missense mutations and one intronic mutation were identified in five microdissected Hodgkin's lymphoma samples. They were not found in the surrounding normal tissues, and thus, were considered as tumour-specific somatic changes.

In total, biallelic *A20* lesions were found in 31 out of 265 lymphoma samples including 3 Hodgkin's lymphoma cell lines. Quantitative analysis of SNP array data suggested that these *A20* lesions were present in the major tumour fraction within the samples (Supplementary Fig. 7). Inactivation of *A20* was most frequent in MALT lymphoma (18 out of 87) and Hodgkin's lymphoma (7 out of 27), although it was also found in DLBCL (5 out of 64) and follicular lymphoma (1 out of 52) at lower frequencies. In MALT lymphoma, biallelic *A20* lesions were confirmed in 18 out of 24 cases (75.0%) with LOH involving the 6q23.3 segment (Supplementary Fig. 8). Considering the limitation in detecting very small homozygous deletions, *A20* was thought to be the target of 6q23 LOH in MALT lymphoma. On the other hand, the 6q23 LOHs in other histology types tended to be extended into more centromeric regions and less frequently accompanied biallelic *A20* lesions (Supplementary Fig. 8 and Supplementary Table 4), indicating that they might be more heterogeneous with regard to their gene targets. We were unable to analyse Hodgkin's lymphoma samples using SNP arrays owing to insufficient genomic DNA obtained from microdissected samples, and were likely to underestimate the frequency of *A20* inactivation in Hodgkin's lymphoma because we might fail to detect a substantial proportion of cases with homozygous deletions, which explained 50% (12 out of 24) of *A20* inactivation in other histology types. *A20* mutations in Hodgkin's lymphoma were exclusively found in nodular sclerosis classical Hodgkin's lymphoma (5 out of 15) but not in other histology types (0 out of 9), although the possible association requires further confirmation in additional cases.

A20 is a key regulator of NF-κB signalling, negatively modulating NF-κB activation through a wide variety of cell surface receptors and viral proteins, including tumour-necrosis factor (TNF) receptors, toll-like receptors, CD40, as well as Epstein–Barr-virus-associated LMP1 protein[2,5,17,18]. To investigate the role of A20 inactivation in lymphomagenesis, we re-expressed wild-type A20 under a *Tet*-inducible promoter in a lymphoma-derived cell line (KM-H2) that had no functional *A20* alleles (Supplementary Fig. 6), and examined the effect of A20 re-expression on cell proliferation, survival and downstream NF-κB signalling pathways. As shown in Fig. 2a–c and Supplementary Fig. 9, re-expression of wild-type A20 resulted in the suppression of cell proliferation and enhanced apoptosis, and in the concomitant accumulation of IκBβ and IκBε, and downregulation of NF-κB activity. In contrast, re-expression of two lymphoma-derived A20 mutants, $A20^{532Stop}$ or $A20^{750Stop}$, failed to show growth suppression, induction of apoptosis, accumulation of IκBβ and IκBε or downregulation of

Table 1 | Inactivation of A20 in B-lineage lymphomas

Histology	Tissue	Sample	Allele	Uniparental disomy	Exon	Mutation	Biallelic inactivation
DLBCL							5 out of 64 (7.8%)
	Lymph node	DLBCL008	−/−	No	−	−	
	Lymph node	DLBCL016	+/−	No	Ex2	329insA	
	Lymph node	DLBCL022	−/−	No	−	−	
	Lymph node	DLBCL028	−/−	Yes	−	−	
	Lymph node	MCL008*	−/−	Yes	−	−	
Follicular lymphoma							1 out of 52 (1.9%)
	Lymph node	FL024	−/−	No	−	−	
MCL							0 out of 35 (0%)
MALT							18 out of 87 (21.8%)
Stomach							3 out of 23 (13.0%)
	Gastric mucosa	MALT013	+/+	Yes	Ex5	705insG	
	Gastric mucosa	MALT014	+/+	Yes	Ex3	Ex3 donor site>A	
	Gastric mucosa	MALT036	+/−	No	Ex7	delintron6–Ex7†	
Eye							13 out of 43 (30.2%)
	Ocular adnexa	MALT008	−/−	No	−	−	
	Ocular adnexa	MALT017	−/−	No	−	−	
	Ocular adnexa	MALT051	+/−	No	Ex7	1943delTG	
	Ocular adnexa	MALT053	+/+	Yes	Ex6	1016G>A(stop)	
	Ocular adnexa	MALT054	+/−	No	Ex3	502delTC	
	Ocular adnexa	MALT055	−/−	No	−	−	
	Ocular adnexa	MALT066	+/−	No	Ex7	1581insA	
	Ocular adnexa	MALT067	−/−	No	−	−	
	Ocular adnexa	MALT082	−/−	Yes	−	−	
	Ocular adnexa	MALT084	−/−	Yes	−	−	
	Ocular adnexa	MALT085	+/+	Yes	Ex7	1435insG	
	Ocular adnexa	MALT086	+/+	Yes	Ex6	878C>T(stop)	
	Ocular adnexa	MALT087	+/+	Yes	Ex9	2304delGG	
Lung							2 out of 12 (16.7%)
	Lung	MALT042	−/−	No	−	−	
	Lung	MALT047	+/+	Yes	Ex9	2281insT	
Other‡							0 out of 9 (0%)
Hodgkin's lymphoma							7 out of 27 (26.0%)
NSHL	Lymph node	HL10	ND	ND	Ex7	1777G>A(V571I)	
NSHL	Lymph node	HL12	ND	ND	Ex7	1156A>G(R364G)	
NSHL	Lymph node	HL21	ND	ND	Ex4	569G>A(stop)	
NSHL	Lymph node	HL24	ND	ND	Ex3	1487C>A(T474N)	
NSHL	Lymph node	HL23	ND	ND	−	Intron 3§	
	Cell line	KM-H2	−/−	No	−		
	Cell line	HDLM2	+/−	No	Ex4	616ins29bp‖	
Total							31 out of 265 (11.7%)

DLBCL, diffuse large B-cell lymphoma; MALT, MALT lymphoma; MCL, mantle cell lymphoma; ND, not determined because SNP array analysis was not performed; NSHL, nodular sclerosis classical Hodgkin's lymphoma.
* Diagnosis was changed based on the genomic data, which was confirmed by re-examination of pathology.
† Deletion including the boundary of intron 6 and exon 7 (see also Supplementary Fig. 5b).
‡ Including 1 parotid gland, 1 salivary gland, 2 colon and 5 thyroid cases.
§ Insertion of CTC at −19 bases from the beginning of exon 3.
‖ Insertion of TGGCTTCCACAGACACACCCATGGCCCGA.

NF-κB activity (Fig. 2a–c), indicating that these were actually loss-of-function mutations. To investigate the role of A20 inactivation in lymphomagenesis *in vivo*, *A20*- and mock-transduced KM-H2 cells were transplanted in NOD/SCID/γ_c^{null} (NOG) mice[19], and their tumour formation status was examined for 5 weeks with or without induction of wild-type A20 by tetracycline administration. As shown in Fig. 2d, mock-transduced cells developed tumours at the injected sites, whereas the *Tet*-inducible *A20*-transduced cells generated tumours only in the absence of A20 induction (Supplementary Table 5), further supporting the tumour suppressor role of A20 in lymphoma development.

Given the mode of negative regulation of NF-κB signalling, we next investigated the origins of NF-κB activity that was deregulated by A20 loss in KM-H2 cells. The conditioned medium prepared from a 48-h serum-free KM-H2 culture had increased NF-κB upregulatory activity compared with fresh serum-free medium, which was inhibited by re-expression of A20 (Fig. 3a). KM-H2 cells secreted two known ligands for TNF receptor—TNF-α and lymphotoxin-α (Supplementary Fig. 10)[20]—and adding neutralizing antibodies against these cytokines into cultures significantly suppressed their cell growth and NF-κB activity without affecting the levels of their overall suppression after A20 induction (Fig. 3b, d). In addition, recombinant TNF-α and/or lymphotoxin-α added to fresh serum-free medium promoted cell growth and NF-κB activation in KM-H2 culture, which were again suppressed by re-expression of A20 (Fig. 3c, e). Although our data in Fig. 3 also show the presence of factors other than TNF-α and lymphotoxin-α in the KM-H2-conditioned medium—as well as some intrinsic pathways in the cell (Fig. 3a)—that were responsible for the A20-dependent NF-κB activation, these results indicate that both cell growth and NF-κB activity that were upregulated by A20 inactivation depend at least partly on the upstream stimuli that evoked the NF-κB-activating signals.

Aberrant activation of the NF-κB pathway is a hallmark of several subtypes of B-lineage lymphomas, including Hodgkin's lymphoma, MALT lymphoma, and a subset of DLBCL, as well as other lymphoid neoplasms[11,14], where a number of genetic alterations of NF-κB signalling pathway genes[21–25], as well as some viral proteins[26,27], have been implicated in the aberrant activation of the NF-κB pathway[14]. Thus, frequent inactivation of A20 in Hodgkin's lymphoma and MALT and other lymphomas provides a novel insight into the molecular pathogenesis of these subtypes of B-lineage lymphomas through deregulated NF-κB activation. Because A20 provides a

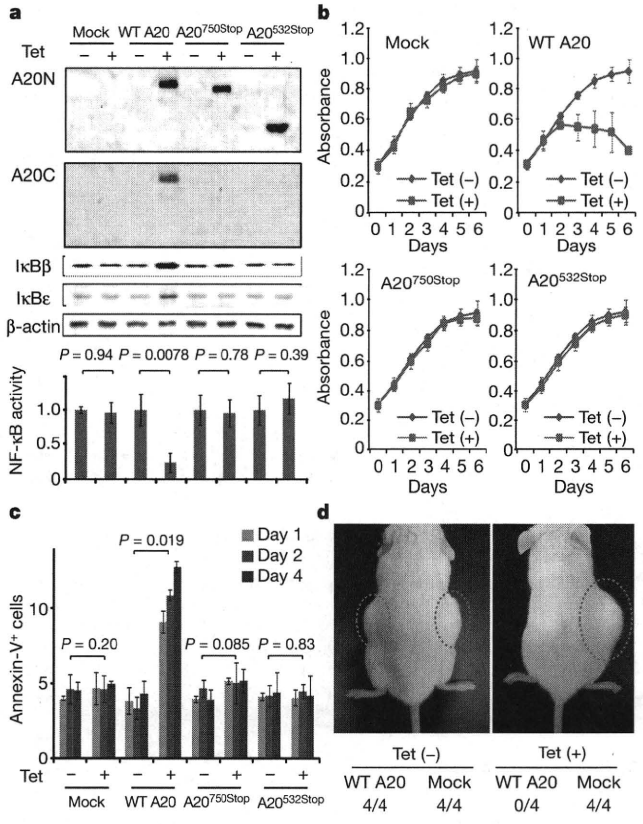

Figure 2 | Effects of wild-type and mutant A20 re-expressed in a lymphoma cell line that lacks the normal *A20* gene. a, Western blot analyses of wild-type (WT) and mutant ($A20^{532Stop}$ and $A20^{750Stop}$) A20, as well as IκBβ and IκBε, in KM-H2 cells, in the presence or absence of tetracycline treatment (top panels). A20N and A20C are polyclonal antisera raised against N-terminal and C-terminal A20 peptides, respectively. β-actin blots are provided as a control. NF-κB activities are expressed as mean absorbance ± s.d. ($n = 6$) in luciferase assays (bottom panel). **b,** Proliferation of KM-H2 cells stably transduced with plasmids for mock and *Tet*-inducible wild-type A20, $A20^{532Stop}$ and $A20^{750Stop}$ was measured using a cell counting kit in the presence (red lines) or absence (blue lines) of tetracycline. Mean absorbance ± s.d. ($n = 5$) is plotted. **c,** The fractions of Annexin-V-positive KM-H2 cells transduced with various *Tet*-inducible A20 constructs were measured by flow cytometry after tetracycline treatment and the mean values (±s.d., $n = 3$) are plotted. **d,** *In vivo* tumorigenicity was assayed by inoculating 7×10^6 KM-H2 cells transduced with mock or *Tet*-inducible wild-type A20 in NOG mice, with (right panel) or without (left panel) tetracycline administration.

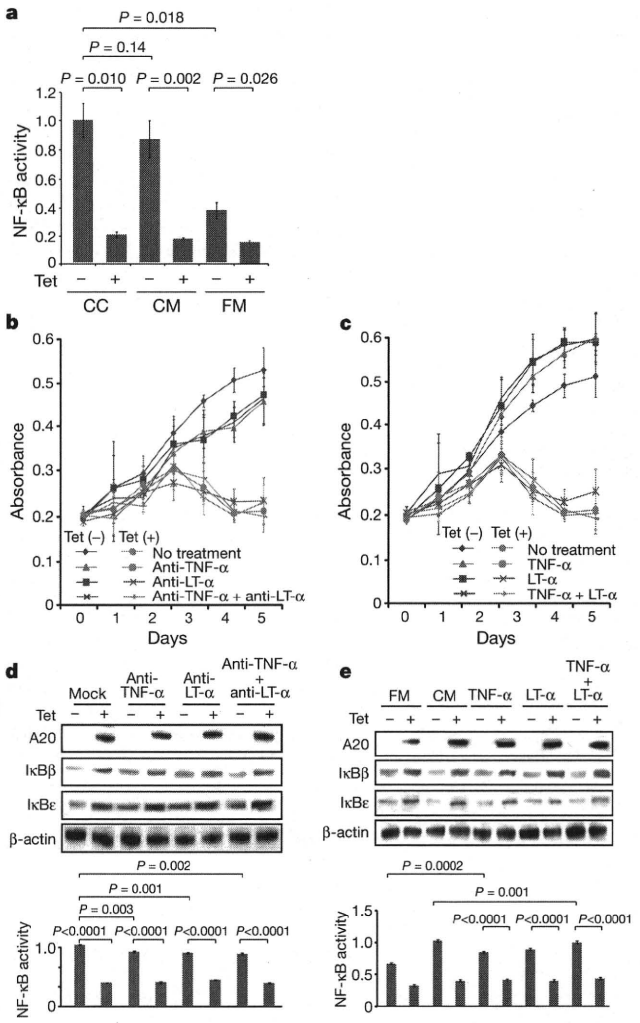

Figure 3 | Tumour suppressor role of A20 under external stimuli. a, NF-κB activity in KM-H2 cells was measured 30 min after cells were inoculated into fresh medium (FM) or KM-H2-conditioned medium (CM) obtained from the 48-h culture of KM-H2, and was compared with the activity after 48 h continuous culture of KM-H2 (CC). A20 was induced 12 h before inoculation in Tet (+) groups. **b, c,** Effects of neutralizing antibodies against TNF-α and lymphotoxin-α (LTα) (**b**) and of recombinant TNF-α and LT-α added to the culture (**c**) on cell growth were evaluated in the presence (Tet (+)) or absence (Tet (−)) of A20 induction. Cell numbers were measured using a cell counting kit and are plotted as their mean absorbance ± s.d. ($n = 6$). **d, e,** Effects of the neutralizing antibodies (**d**) and the recombinant cytokines added to the culture (**e**) on NF-κB activities and the levels of IκBβ and IκBε after 48 h culture with (Tet (+)) or without (Tet (−)) tetracycline treatment. NF-κB activities are expressed as mean absorbance ± s.d. ($n = 6$) in luciferase assays.

negative feedback mechanism in the regulation of NF-κB signalling pathways upon a variety of stimuli, aberrant activation of NF-κB will be a logical consequence of A20 inactivation. However, there is also the possibility that the aberrant NF-κB activity of A20-inactivated lymphoma cells is derived from upstream stimuli, which may be from the cellular environment. In this context, it is intriguing that MALT lymphoma usually arises at the site of chronic inflammation caused by infection or autoimmune disorders and may show spontaneous regression after eradication of infectious organisms[28]; furthermore, Hodgkin's lymphoma frequently shows deregulated cytokine production from Reed–Sternberg cells and/or surrounding reactive cells[29]. Detailed characterization of the NF-κB pathway regulated by A20 in both normal and neoplastic B lymphocytes will promote our understanding of the precise roles of A20 inactivation in the pathogenesis of these lymphoma types. Our finding underscores the importance of genome-wide approaches in the identification of genetic targets in human cancers.

METHODS SUMMARY

Genomic DNA from 238 patients with non-Hodgkin's lymphoma and three Hodgkin's-lymphoma-derived cell lines was analysed using GeneChip SNP genotyping microarrays (Affymetrix). This study was approved by the ethics boards of the University of Tokyo, National Cancer Institute Hospital, Okayama University, and the Cancer Institute of the Japanese Foundation of Cancer Research. After appropriate normalization of mean array intensities, signal ratios between tumours and anonymous normal references were calculated in an allele-specific manner, and allele-specific copy numbers were inferred from the observed signal ratios based on the hidden Markov model using CNAG/AsCNAR software (http://www.genome.umin.jp). *A20* mutations were examined by directly sequencing genomic DNA using a set of primers (Supplementary Table 6). Full-length cDNAs of wild-type and mutant *A20* were introduced into a

lentivirus vector, pLenti4/TO/V5-DEST (Invitrogen), with a *Tet*-inducible promoter. Viral stocks were prepared by transfecting the vector plasmids into 293FT cells (Invitrogen) using the calcium phosphate method and then infected to the KM-H2 cell line. Proliferation of KM-H2 cells was measured using a Cell Counting Kit (Dojindo). Western blot analyses and luciferase assays were performed as previously described. NF-κB activity was measured by luciferase assays in KM-H2 cells stably transduced with a reporter plasmid having an NF-κB response element, pGL4.32 (Promega). Apoptosis of KM-H2 upon A20 induction was evaluated by counting Annexin-V-positive cells by flow cytometry. For *in vivo* tumorigenicity assays, 7×10^6 KM-H2 cells were transduced with the *Tet*-inducible *A20* gene and those with a mock vector were inoculated on the contralateral sides in eight NOG mice[19] and examined for their tumour formation with ($n = 4$) or without ($n = 4$) tetracycline administration. Full copy number data of the 238 lymphoma samples will be accessible from the Gene Expression Omnibus (GEO, http://ncbi.nlm.nih.gov/geo/) with the accession number GSE12906.

Full Methods and any associated references are available in the online version of the paper at www.nature.com/nature.

Received 17 September 2008; accepted 3 March 2009.
Published online 3 May 2009.

1. Dixit, V. M. *et al.* Tumor necrosis factor-α induction of novel gene products in human endothelial cells including a macrophage-specific chemotaxin. *J. Biol. Chem.* **265,** 2973–2978 (1990).
2. Song, H. Y., Rothe, M. & Goeddel, D. V. The tumor necrosis factor-inducible zinc finger protein A20 interacts with TRAF1/TRAF2 and inhibits NF-κB activation. *Proc. Natl Acad. Sci. USA* **93,** 6721–6725 (1996).
3. Lee, E. G. *et al.* Failure to regulate TNF-induced NF-κB and cell death responses in A20-deficient mice. *Science* **289,** 2350–2354 (2000).
4. Boone, D. L. *et al.* The ubiquitin-modifying enzyme A20 is required for termination of Toll-like receptor responses. *Nature Immunol.* **5,** 1052–1060 (2004).
5. Wang, Y. Y., Li, L., Han, K. J., Zhai, Z. & Shu, H. B. A20 is a potent inhibitor of TLR3- and Sendai virus-induced activation of NF-κB and ISRE and IFN-β promoter. *FEBS Lett.* **576,** 86–90 (2004).
6. Wertz, I. E. *et al.* De-ubiquitination and ubiquitin ligase domains of A20 downregulate NF-κB signalling. *Nature* **430,** 694–699 (2004).
7. Heyninck, K. & Beyaert, R. A20 inhibits NF-κB activation by dual ubiquitin-editing functions. *Trends Biochem. Sci.* **30,** 1–4 (2005).
8. Graham, R. R. *et al.* Genetic variants near *TNFAIP3* on 6q23 are associated with systemic lupus erythematosus. *Nature Genet.* **40,** 1059–1061 (2008).
9. Musone, S. L. *et al.* Multiple polymorphisms in the *TNFAIP3* region are independently associated with systemic lupus erythematosus. *Nature Genet.* **40,** 1062–1064 (2008).
10. Jaffe, E. S., Harris, N. L., Stein, H. & Vardiman, J. W. *World Health Organization Classification of Tumours. Pathology and Genetics of Tumours of Hematopoietic and Lymphoid Tissues* (IARC Press, 2001).
11. Klein, U. & Dalla-Favera, R. Germinal centres: role in B-cell physiology and malignancy. *Nature Rev. Immunol.* **8,** 22–33 (2008).
12. Nannya, Y. *et al.* A robust algorithm for copy number detection using high-density oligonucleotide single nucleotide polymorphism genotyping arrays. *Cancer Res.* **65,** 6071–6079 (2005).
13. Yamamoto, G. *et al.* Highly sensitive method for genomewide detection of allelic composition in nonpaired, primary tumor specimens by use of affymetrix single-nucleotide-polymorphism genotyping microarrays. *Am. J. Hum. Genet.* **81,** 114–126 (2007).
14. Jost, P. J. & Ruland, J. Aberrant NF-κB signaling in lymphoma: mechanisms, consequences, and therapeutic implications. *Blood* **109,** 2700–2707 (2007).
15. Durkop, H., Hirsch, B., Hahn, C., Foss, H. D. & Stein, H. Differential expression and function of A20 and TRAF1 in Hodgkin lymphoma and anaplastic large cell lymphoma and their induction by CD30 stimulation. *J. Pathol.* **200,** 229–239 (2003).
16. Honma, K. *et al. TNFAIP3* is the target gene of chromosome band 6q23.3-q24.1 loss in ocular adnexal marginal zone B cell lymphoma. *Genes Chromosom. Cancer* **47,** 1–7 (2008).
17. Sarma, V. *et al.* Activation of the B-cell surface receptor CD40 induces A20, a novel zinc finger protein that inhibits apoptosis. *J. Biol. Chem.* **270,** 12343–12346 (1995).
18. Fries, K. L., Miller, W. E. & Raab-Traub, N. The A20 protein interacts with the Epstein-Barr virus latent membrane protein 1 (LMP1) and alters the LMP1/TRAF1/TRADD complex. *Virology* **264,** 159–166 (1999).
19. Hiramatsu, H. *et al.* Complete reconstitution of human lymphocytes from cord blood $CD34^+$ cells using the NOD/SCID/γ^{null} mice model. *Blood* **102,** 873–880 (2003).
20. Hsu, P. L. & Hsu, S. M. Production of tumor necrosis factor-α and lymphotoxin by cells of Hodgkin's neoplastic cell lines HDLM-1 and KM-H2. *Am. J. Pathol.* **135,** 735–745 (1989).
21. Dierlamm, J. *et al.* The apoptosis inhibitor gene *API2* and a novel 18q gene, *MLT*, are recurrently rearranged in the t(11;18)(q21;q21) associated with mucosa-associated lymphoid tissue lymphomas. *Blood* **93,** 3601–3609 (1999).
22. Willis, T. G. *et al.* Bcl10 is involved in t(1;14)(p22;q32) of MALT B cell lymphoma and mutated in multiple tumor types. *Cell* **96,** 35–45 (1999).
23. Joos, S. *et al.* Classical Hodgkin lymphoma is characterized by recurrent copy number gains of the short arm of chromosome 2. *Blood* **99,** 1381–1387 (2002).
24. Martin-Subero, J. I. *et al.* Recurrent involvement of the *REL* and *BCL11A* loci in classical Hodgkin lymphoma. *Blood* **99,** 1474–1477 (2002).
25. Lenz, G. *et al.* Oncogenic *CARD11* mutations in human diffuse large B cell lymphoma. *Science* **319,** 1676–1679 (2008).
26. Deacon, E. M. *et al.* Epstein-Barr virus and Hodgkin's disease: transcriptional analysis of virus latency in the malignant cells. *J. Exp. Med.* **177,** 339–349 (1993).
27. Yin, M. J. *et al.* HTLV-I Tax protein binds to MEKK1 to stimulate IκB kinase activity and NF-κB activation. *Cell* **93,** 875–884 (1998).
28. Isaacson, P. G. & Du, M. Q. MALT lymphoma: from morphology to molecules. *Nature Rev. Cancer* **4,** 644–653 (2004).
29. Skinnider, B. F. & Mak, T. W. The role of cytokines in classical Hodgkin lymphoma. *Blood* **99,** 4283–4297 (2002).

Supplementary Information is linked to the online version of the paper at www.nature.com/nature.

Acknowledgements This work was supported by the Core Research for Evolutional Science and Technology, Japan Science and Technology Agency, by the 21st century centre of excellence program 'Study on diseases caused by environment/genome interactions', and by Grant-in-Aids from the Ministry of Education, Culture, Sports, Science and Technology of Japan and from the Ministry of Health, Labor and Welfare of Japan for the 3rd-term Comprehensive 10-year Strategy for Cancer Control. We also thank Y. Ogino, E. Matsui and M. Matsumura for their technical assistance.

Author Contributions M.Ka., K.N. and M.S. performed microarray experiments and subsequent data analyses. M.Ka., Y.C., K.Ta., J.T., J.N., M.I., A.T. and Y.K. performed mutation analysis of *A20*. M.Ka., S.Mu., M.S., Y.C. and Y.Ak. conducted functional assays of mutant A20. Y.S., K.Ta., Y.As., H.M., M.Ku., S.Mo., S.C., Y.K., K.To. and Y.I. prepared tumour specimens. I.K., K.O., A.N., H.N. and T.N. conducted *in vivo* tumorigenicity experiments in NOG/SCID mice. T.I., Y.H., T.Ÿ., Y.K. and S.O. designed overall studies, and S.O. wrote the manuscript. All authors discussed the results and commented on the manuscript.

Author Information The copy number data as well as the raw microarray data will be accessible from the GEO (http://ncbi.nlm.nih.gov/geo/) with the accession number GSE12906. Reprints and permissions information is available at www.nature.com/reprints. Correspondence and requests for materials should be addressed to S.O. (sogawa-tky@umin.ac.jp) or Y.K. (ykkobaya@ncc.go.jp).